Unified modular state-space modeling of grid-connected voltage-source converters

Unified Modular State-Space Modeling of Grid-Connected Voltage-Source Converters

Dongsheng Yang, *Senior Member*, *IEEE*, Xiongfei Wang, *Senior Member*, *IEEE*

***Abstract*—This paper proposes a modular state-space modeling framework for grid-connected voltage-source converters, where the different control loops, including the ac current control, the phase-locked loop, the dc-link voltage control and the ac voltage magnitude control, can be modeled separately as building blocks. Moreover, the mathematical relationship between state-space models in the rotating (*dq*-) frame and the stationary ($\alpha\beta$-) frame are explicitly established, and thus the modal analysis can be performed directly in the $\alpha\beta$-frame, which allows intuitive interpretation of voltage and current oscillation modes in the $\alpha\beta$-frame. Experimental tests of a 3 kW back-to-back converter system validate the effectiveness of the unified modular state-space modeling and analysis.**

***Index Terms*—state-space model, component connection method, sensitivity analysis, frequency coupling, stationary frame**

I. Introduction

Voltage-Source Converters (VSCs) are widely used in power grid applications, e.g. renewable power generations [1], flexible power transmission and distributions, as well as energy-efficient consumptions [2]-[3]. The ever-increasing use of VSCs brings in more control flexibility and improved efficiency, but does also pose a number of new challenges to stability and power quality of the power system [4].

Many research efforts have thus been made to address VSC-grid interactions. The impedance-based modeling approach has been recently reported in [5], [6] to analyze the dynamic effects of different control loops on the VSC-grid interactions. For the inner current loop, the multiple-input multiple-output (MIMO) system model can be simplified into single-input single-output (SISO) transfer functions based on complex space vectors. This SISO impedance model not only provides an intuitive insight into the interactions among the paralleled VSCs and weak power grids, but also enables to reshape the output impedances of VSCs for stabilizing the power system [7]-[8].

However, the frequency coupling effects will be induced by the inherent asymmetry of the outer control loops, such as the phase-locked loop (PLL), the dc-link voltage control (DVC), and the ac voltage magnitude control (AVC), which significantly complicate the analysis of converter dynamics. Instead of the SISO impedance transfer function, the impedance matrix has to be used to model the terminal dynamics of converters [9]-[11]. Consequently, the Generalized Nyquist Criterion (GNC) is utilized for the stability assessment, and the stability analysis results usually provide little insight into the controller design and the system damping.

To facilitate the controller design-oriented analysis, research works on transforming the MIMO impedance model as a closed-loop SISO system have been reported recently [12]. However, the approach requires prior knowledge on the grid impedance, which is varying over time in practice and it is difficult to predict.

Alternatively, the state-space modeling and modal analysis can also be employed to design controllers for stabilizing VSC-grid interactions [13]. The eigenvalues and eigenvectors of the state matrix provide a complete overview of the system oscillatory modes and their damping factors [14]. The participation factors and sensitivity analysis further reveal the dynamic contributions of state variables and system parameters, and thus help to identify the root causes of critical oscillations [15]. Moreover, differing from the impedance-based analysis, which reflects the input-output dynamic relationship locally, the state-space modeling gives a global view of the system dynamics and is thus generally preferred for large-scale interconnected systems [16].

In spite of the advantages of the modal analysis, the basic state-space modeling approach features less modularity and scalability than the impedance-based method, with respect to analyzing the control impacts of VSCs [17]. Moreover, the nonlinear dynamics of the outer control loops and the PLL adds more interconnections among control loops [18]-[20], which complicate the derivation of the state matrix of the whole control system.

To simplify the modeling process, many efforts have been devoted to modularize the state-space modeling method. In [21], each control loop of the VSC is modeled separately as a sub-state-space model, and then the models are combined together based on their interconnections. However, there are shared state variables among sub-state-space models, which have to be merged together to obtain the right state variables for the state matrix of the overall system. Therefore, without a clear definition of the combination rule, considerable efforts are needed to reformulate the sub-state-space models for them to be incorporated into the system model. Hence, to tackle this challenge, the rules for combining two sub-state-space models with different interconnection forms, i.e., the parallel, the concatenation, the feedback, and the common input or output, are introduced in [22]. The shared state variables can be represented by a single state variable with interconnections between the sub-modules. Thus, the overall system model can be readily derived without the reformulations of sub-state-space models. Those rules only apply to two subsystems with a well-defined interconnection form, whereas the control loops of VSCs are cross-coupled with each other, which makes those rules difficult to apply.

Another modular state-space modeling approach that has been applied to power systems is the component connection method (CCM) [23], where the system is decomposed into multiple components, whose interconnections are modeled as a linear algebra matrix based on the algebraic relations of their inputs and outputs. Thus, the system state-space model can be obtained by combining the linear algebra matrix with the individual state-space models of components [24]. This

Manuscript received Sep. 06, 2019; revised Dec. 13, 2019; accepted Jan. 04, 2020. *(Corresponding author: Xiongfei Wang)*

D. Yang is with the Department of Electrical Engineering, Eindhoven Univerisity of Technology, Eindhoven, Netherlands (e-mail: d.yang1@tue.nl).

X. Wang is with the Department of Energy Technology, Aalborg University, Aalborg, Denmark (e-mail: xwa@et.aau.dk).

method features better modularity and scalability than that reported in [22], and remarkably reduces the computational effort for the power networks where the interconnections of equipment can be explicitly defined. However, the CCM is still not readily used for modeling the control loops of VSCs, since the linearization of the outer control loops introduces additional sub-state-space models and interconnections, which are implicit as opposed to the physical sub-state-space model and interconnections. Therefore, a modular state-space modeling method that can characterize the effects of control loops is still missing.

Besides the modeling complexity, another obstacle that impedes the widespread use of the state-space modeling method is the lack of a unified mathematical relationship between the state-space models in different reference frames.

To obtain the time-invariant operating point, the state-space models of VSCs are generally developed in the *dq*-frame [25]. However, with the *dq*-frame state-space model, it is difficult to link the oscillation modes in the *dq*-frame to actual oscillation modes in the *αβ*-frame. The relations between the oscillation modes in the two frames can be either frequency-shifted, e.g. the symmetric *dq*-frame current control, or frequency-coupled, e.g. the asymmetric *dq*-frame dynamics of the PLL [11], [26]-[27]. It is worth noting that this limitation of the *dq*-frame state-space model is also imposed on the *dq*-frame impedance model, and recent studies have thus been devoted to developing the *αβ* impedance model [28]-[29]. In [27], the unified impedance model is introduced which bridges the mathematical relationships between the impedance models in the *dq*- and *αβ*-frames. It is shown that the *αβ*-frame impedance-based analysis can explicitly reveal the frequency-couplings between the sub- and super-synchronous oscillations. However, the *αβ*- frame state-space model of VSCs still remains an open issue.

To address the abovementioned challenges, this study provides an improved modular state-space modeling framework as compared with [23], which enables to model the system with implicit sub-systems and connections caused by linearization of control loops. Another major contribution of this study is to establish the mathematical relationship between the state-space models in the *dq*-frame and the *αβ*-frame, which allows the straightforward stability analysis and intuitive interpretation of voltage and current oscillation modes in the *αβ*-frame.

The remainder of the paper is organized as follows: Section II describes the configuration of the studied system, and also proposes the improved framework of modular state-space modeling. The sub-state-space models and interconnections used in the framework are derived in Section III and IV. Based on which, the system state-space model is established firstly in the *dq*-frame in Section V, and the mathematical relationships between the state-space models in the *dq*- and *αβ*-frames are proposed in Section VI. Then the stability analysis based on the unified state-space model is presented in Section VII. Lastly, experimental tests on a 3 kW back-to-back converter system are conducted to validate the effectiveness of the unified modular state-space modeling approach in Section VIII, and Section IX concludes the paper.

II. System Description And Modeling Method

A. System Configuration

The control scheme of the grid-connected VSC is shown in Fig. 1. Basically, the control scheme can be divided into four parts, including the AC current control (ACC), Phase-locked-loop (PLL), dc-link voltage control (DVC), and AC voltage magnitude control (AVC). C_{dc} is the dc-link capacitor; L_1 is the converter filter inductor; C_g and L_g are equivalent grid capacitance and grid inductance seen from point of common connection (PCC).

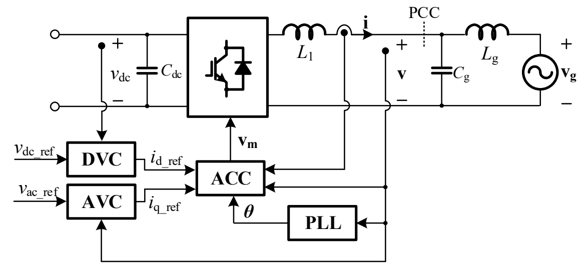

Fig. 1. The control scheme of the grid-connected VSC

As shown in [8], the real space vectors are usually denoted with italic letters, e.g., $x_{dq} = [x_d, x_q]^T$, while complex space vectors are denoted with boldface letters, e.g., $\mathbf{x_{dq}} = x_d + jx_q$, $\mathbf{x_{dq}}^* = x_d - jx_q$. To avoid the confusion between real space vector (such as x_{dq}) and scalar (such as x_d), the vectors in this paper are accented with a right arrow, i.e., $\vec{x}_{dq} = \left[x_d, x_q\right]^T$ and $\vec{\mathbf{X}}_{\mathbf{dq}} = \left[\mathbf{x_{dq}}, \mathbf{x_{dq}^*}\right]^T$.

In Fig. 1, the complex space vectors of converter output current and voltage are denoted by **i** and **v** respectively, while the compelx space vector of grid voltage is denoted by $\mathbf{v_g}$.

B. Modular State-Space Modeling Method

The flow chart of the CCM based modular state-space modeling is shown in Fig. 2(a). Firstly, the system can be portioned to *n* sub-systems. Then the sub-systems are modeled separately. Assuming that the sub-state-space model of i^{th} component can be given by a set of nonlinear equations as follows:

$$\dot{\vec{x}}_i = f_i\left(\vec{x}_i, \vec{a}_i\right) \tag{1a}$$

$$\vec{b}_i = g_i\left(\vec{x}_i, \vec{a}_i\right) \tag{1b}$$

where $\vec{x}_i$, $\vec{a}_i$ and $\vec{b}_i$ denotes the state variables, input variables, and output variables. The small-signal state-space model of the i^{th} component can be obtained by linearizing (1)

$$\Delta\dot{\vec{x}}_i = F_i\Delta\vec{x}_i + H_i\Delta\vec{a}_i \tag{2a}$$

$$\Delta\vec{b}_i = J_i\Delta\vec{x}_i + K_i\Delta\vec{a}_i \tag{2b}$$

For simplicity, the prefixes Δ in (2) are disregarded in the following.

Moreover, the interconnections among different components have to be obtained and expressed by algebraic equations as

$$\vec{a} = L_1\vec{b} + L_2\vec{u} \tag{3a}$$

$$\vec{y} = L_3\vec{b} + L_4\vec{u} \tag{3b}$$

where $\vec{a} = \left[\vec{a}_1, \ldots \vec{a}_i, \ldots \vec{a}_n\right]^T$ and $\vec{b} = \left[\vec{b}_1, \ldots \vec{b}_i, \ldots \vec{b}_n\right]^T$ are input and output vectors of all components; $\vec{u}$ and $\vec{y}$ are system input and output vectors. L_1, L_2, L_3, and L_4 are parameter matrices that map the interconnection relationships among different components.

The combination rule for obtaining the system state-space model can be given as follows:

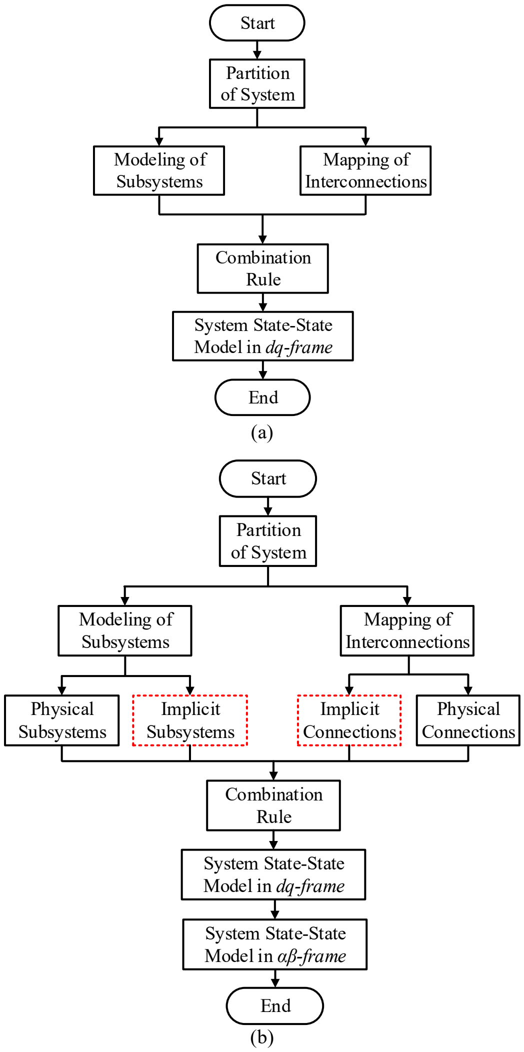

Fig. 2. Modular State-space modeling methods (a) conventional CCM method (b) Proposed method

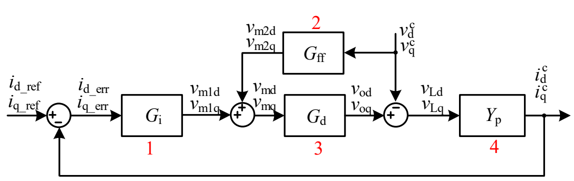

Fig. 3. Block diagram of the current control in the converter dq-frame without considering the PLL dynamics.

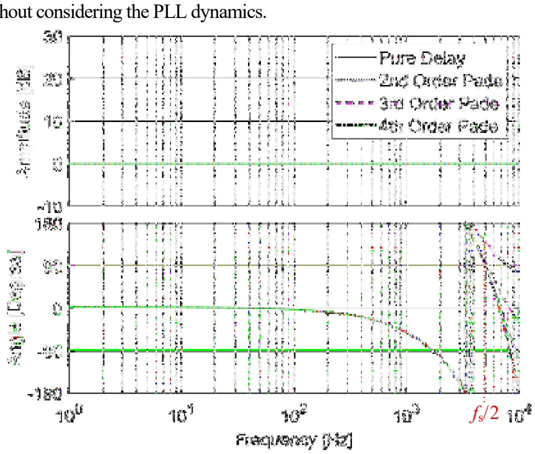

Fig. 4. Comparison of Pade approximations with different orders

The composite system model can be formulated by combining all the sub-state-space models of components

$$\dot{\vec{x}} = F\vec{x} + H\vec{a} \tag{4a}$$

$$\vec{b} = J\vec{x} + K\vec{a} \tag{4b}$$

where F, H, J, K are the diagonal parameter matrices of the composite system model, F=diag(F_1,… F_i, … F_n), H=diag(H_1,… H_i, … H_n), J=diag(J_1,… J_i, … J_n), K=diag(K_1,… K_i, … K_n); $\vec{x} = \left[\vec{x}_1, \ldots \vec{x}_i, \ldots \vec{x}_n\right]^T$.

Then, the overall state-space model of the system can be expressed as:

$$\dot{\vec{x}} = A\vec{x} + B\vec{u} \tag{5a}$$

$$\vec{y} = C\vec{x} + D\vec{u} \tag{5b}$$

where A, B, C, D are the parameter matrices of the overall state-space model of the system, which are expressed as.

$$A = F + HL_1\left(I - KL_1\right)^{-1} J \tag{6a}$$

$$B = HL_1\left(I - KL_1\right)^{-1} KL_2 + HL_2 \tag{6b}$$

$$C = L_3\left(I - KL_1\right)^{-1} J \tag{6c}$$

$$D = L_3\left(I - KL_1\right)^{-1} KL_2 + L_4 \tag{6d}$$

where I is the identity matrix with the same dimension as KL_1.

However, the traditional CCM based modular state-space modeling method can only be applied to the system where the interconnections among its sub-systems can be explicitly defined. Therefore, a modular state-space modeling method is developed in this work to deal with implicit sub-state space models and interconnections which are introduced by linearizing of the outer loops, as shown in Fig. 2(b). Moreover, mathematical relationships between the system-state-space model in the dq-frame and that in the $\alpha\beta$-frame are also incorporated to facilitate the system stability analysis.

III. Physical Sub-State-Space Models

A. AC Current Control

The block diagram of the current control in the converter dq-frame without considering the PLL dynamics is shown in Fig. 3, which contains the current controller G_i, the voltage feedforward controller G_{ff}, the control delay G_d, and the admittance of L filter Y_p. i_{d/q_ref}, i_{d/q_err} are the current reference and error, respectively; $v_{m1d/q}$, $v_{m2d/q}$, $v_{md/q}$ are modulating signals generated by the current control, the feedforward controller and their sum; $v_{od/q}$, $v_{Ld/q}$ are converter output voltages and the inductor voltages, respectively; $v_{d/q}^c$, $i_{d/q}^c$ are the voltage and current at the PCC of VSC, respectively; All these variables are defined in the converter dq-frame.

Since the ACC contains multiple components, the CCM will be employed to establish its state-space model. For a clear illustration, G_i, G_{ff}, G_d, and Y_p will be denoted as component 1 to 4, respectively.

The current controller $G_i(s)$ adopts PI controller, given by

$$G_i(s) = k_{pc} + \frac{k_{ic}}{s} \tag{7}$$

Active damping is implemented by a first-order High-

Pass Filter (HPF) based feedforward control, express as:

$$G_{\mathrm{ff1}}(s)=\frac{k_{\mathrm{a}}s}{s+\omega_{\mathrm{a}}} \tag{8}$$

The HPF is chosen because it can be equivalently treated as a virtual parallel resistor at the PCC within the corner-frequency of HPF [30], which helps to improve the stability of the system.

With the digital control, the computation and pulse-width modulation (PWM) will introduce the control delay, which can be expressed as:

$$G_{\mathrm{d}}(s)=e^{-sT_{\mathrm{d}}} \tag{9}$$

where T_{d} is the delay time, which is typically 1.5 times of sampling period T_{s}, i.e., $T_{\mathrm{d}}=1.5T_{\mathrm{s}}$. To get the adequate state-space model of the control delay, the third-order Pade approximation is applied to make the model sufficiently accurate within Nyquist frequency, i.e., half of the sampling frequency, and meanwhile minimize the complexity, as shown in Fig. 4, which is expressed as

$$G_{\mathrm{d}}(s)=e^{-sT_{\mathrm{d}}}\approx\frac{120-60T_{\mathrm{d}}s+12\left(T_{\mathrm{d}}s\right)^{2}-\left(T_{\mathrm{d}}s\right)^{3}}{120+60T_{\mathrm{d}}s+12\left(T_{\mathrm{d}}s\right)^{2}+\left(T_{\mathrm{d}}s\right)^{3}} \tag{10}$$

The admittance of L filter in the converter dq-frame can be given by:

$$Y_{\mathrm{p}}(s)=\frac{1}{\left(s+j\omega_{1}\right)L_{1}+R_{1}} \tag{11}$$

where ω_1 is the nominal angular frequency of the grid, and R_1 is the equivalent series resistor (ESR).

Since all the components in ACC are linear, their state-space models can be directly obtained according to their transfer-functions, where the details are presented in the Appendix A. With these sub-state-space models denoted by subscript from 1 to 4, the composite model of ACC can be obtained by rearranging these matrices in a diagonal form, which is expressed as

$$\underbrace{\begin{bmatrix}\dot{\vec{x}}_1\\ \dot{\vec{x}}_2\\ \dot{\vec{x}}_3\\ \dot{\vec{x}}_4\end{bmatrix}}_{\dot{\vec{x}}_{\mathrm{acc}}}=\underbrace{\begin{bmatrix}F_1&&&\\&F_2&&\\&&F_3&\\&&&F_4\end{bmatrix}}_{F_{\mathrm{acc}}}\underbrace{\begin{bmatrix}\vec{x}_1\\ \vec{x}_2\\ \vec{x}_3\\ \vec{x}_4\end{bmatrix}}_{\vec{x}_{\mathrm{acc}}}+\underbrace{\begin{bmatrix}H_1&&&\\&H_2&&\\&&H_3&\\&&&H_4\end{bmatrix}}_{H_{\mathrm{acc}}}\underbrace{\begin{bmatrix}\vec{a}_1\\ \vec{a}_2\\ \vec{a}_3\\ \vec{a}_4\end{bmatrix}}_{\vec{a}_{\mathrm{acc}}} \tag{12a}$$

$$\underbrace{\begin{bmatrix}\vec{b}_1\\ \vec{b}_2\\ \vec{b}_3\\ \vec{b}_4\end{bmatrix}}_{\vec{b}_{\mathrm{acc}}}=\underbrace{\begin{bmatrix}J_1&&&\\&J_2&&\\&&J_3&\\&&&J_4\end{bmatrix}}_{J_{\mathrm{acc}}}\underbrace{\begin{bmatrix}\vec{x}_1\\ \vec{x}_2\\ \vec{x}_3\\ \vec{x}_4\end{bmatrix}}_{\vec{x}_{\mathrm{acc}}}+\underbrace{\begin{bmatrix}K_1&&&\\&K_2&&\\&&K_3&\\&&&K_4\end{bmatrix}}_{K_{\mathrm{acc}}}\underbrace{\begin{bmatrix}\vec{a}_1\\ \vec{a}_2\\ \vec{a}_3\\ \vec{a}_4\end{bmatrix}}_{\vec{a}_{\mathrm{acc}}} \tag{12b}$$

where the expressions of matrices F_1, H_1, J_1, K_1 are defined in (A1); F_2, H_2, J_2, K_2 in (A2); F_3, H_3, J_3, K_3 in (A3); and F_4, H_4, J_4, K_4 in (A6).

According to Fig. 3, the input vector $\vec{a}_{\mathrm{acc}}$ and output vector $\vec{b}_{\mathrm{acc}}$ in (12) can be expanded as:

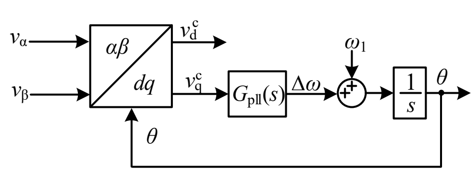

Fig. 5. Block diagram of the SRF-PLL

$$\vec{a}_{\mathrm{acc}}=\begin{bmatrix}\vec{a}_1\\ \vec{a}_2\\ \vec{a}_3\\ \vec{a}_4\end{bmatrix}=\begin{bmatrix}i_{\mathrm{d\_err}}\\ i_{\mathrm{q\_err}}\\ v_{\mathrm{d}}^{\mathrm{c}}\\ v_{\mathrm{q}}^{\mathrm{c}}\\ v_{\mathrm{md}}\\ v_{\mathrm{mq}}\\ v_{\mathrm{Ld}}\\ v_{\mathrm{Lq}}\end{bmatrix}\qquad \vec{b}_{\mathrm{acc}}=\begin{bmatrix}\vec{b}_1\\ \vec{b}_2\\ \vec{b}_3\\ \vec{b}_4\end{bmatrix}=\begin{bmatrix}v_{\mathrm{m1d}}\\ v_{\mathrm{m1q}}\\ v_{\mathrm{m2d}}\\ v_{\mathrm{m2q}}\\ v_{\mathrm{od}}\\ v_{\mathrm{oq}}\\ i_{\mathrm{d}}^{\mathrm{c}}\\ i_{\mathrm{q}}^{\mathrm{c}}\end{bmatrix} \tag{13}$$

The input vector $\vec{u}_{\mathrm{acc}}$ and output vector $\vec{y}_{\mathrm{acc}}$ of overall ACC are expressed as

$$\vec{u}_{\mathrm{acc}}=\begin{bmatrix}i_{\mathrm{d\_ref}}\\ i_{\mathrm{q\_ref}}\\ v_{\mathrm{d}}^{\mathrm{c}}\\ v_{\mathrm{q}}^{\mathrm{c}}\end{bmatrix}\qquad \vec{y}_{\mathrm{acc}}=\begin{bmatrix}i_{\mathrm{d}}^{\mathrm{c}}\\ i_{\mathrm{q}}^{\mathrm{c}}\end{bmatrix} \tag{14}$$

Consequently, the physical interconnection among different components in Fig. 3 can be depicted by

$$\underbrace{\begin{bmatrix}i_{\mathrm{d\_err}}\\ i_{\mathrm{q\_err}}\\ v_{\mathrm{d}}^{\mathrm{c}}\\ v_{\mathrm{q}}^{\mathrm{c}}\\ v_{\mathrm{md}}\\ v_{\mathrm{mq}}\\ v_{\mathrm{Ld}}\\ v_{\mathrm{Lq}}\end{bmatrix}}_{\vec{a}_{\mathrm{acc}}}=\underbrace{\begin{bmatrix}0&0&0&0&0&0&-1&0\\0&0&0&0&0&0&0&-1\\0&0&0&0&0&0&0&0\\0&0&0&0&0&0&0&0\\1&0&1&0&0&0&0&0\\0&1&0&1&0&0&0&0\\0&0&0&0&1&0&0&0\\0&0&0&0&0&1&0&0\end{bmatrix}}_{L_{\mathrm{acc1}}}\underbrace{\begin{bmatrix}v_{\mathrm{m1d}}\\ v_{\mathrm{m1q}}\\ v_{\mathrm{m2d}}\\ v_{\mathrm{m2q}}\\ v_{\mathrm{od}}\\ v_{\mathrm{oq}}\\ i_{\mathrm{d}}^{\mathrm{c}}\\ i_{\mathrm{q}}^{\mathrm{c}}\end{bmatrix}}_{\vec{b}_{\mathrm{acc}}}+\underbrace{\begin{bmatrix}1&0&0&0\\0&1&0&0\\0&0&1&0\\0&0&0&1\\0&0&0&0\\0&0&0&0\\0&0&-1&0\\0&0&0&-1\end{bmatrix}}_{L_{\mathrm{acc2}}}\underbrace{\begin{bmatrix}i_{\mathrm{d\_ref}}\\ i_{\mathrm{q\_ref}}\\ v_{\mathrm{d}}^{\mathrm{c}}\\ v_{\mathrm{q}}^{\mathrm{c}}\end{bmatrix}}_{\vec{u}_{\mathrm{acc}}} \tag{15a}$$

$$\underbrace{\begin{bmatrix}i_{\mathrm{d}}^{\mathrm{c}}\\ i_{\mathrm{q}}^{\mathrm{c}}\end{bmatrix}}_{\vec{y}_{\mathrm{acc}}}=\underbrace{\begin{bmatrix}0&0&0&0&0&0&1&0\\0&0&0&0&0&0&0&1\end{bmatrix}}_{L_{\mathrm{acc3}}}\underbrace{\begin{bmatrix}v_{\mathrm{m1d}}\\ v_{\mathrm{m1q}}\\ v_{\mathrm{m2d}}\\ v_{\mathrm{m2q}}\\ v_{\mathrm{od}}\\ v_{\mathrm{oq}}\\ i_{\mathrm{d}}^{\mathrm{c}}\\ i_{\mathrm{q}}^{\mathrm{c}}\end{bmatrix}}_{\vec{b}_{\mathrm{acc}}}+\underbrace{\begin{bmatrix}0&0&0&0\\0&0&0&0\end{bmatrix}}_{L_{\mathrm{acc4}}}\underbrace{\begin{bmatrix}i_{\mathrm{d\_ref}}\\ i_{\mathrm{q\_ref}}\\ v_{\mathrm{d}}^{\mathrm{c}}\\ v_{\mathrm{q}}^{\mathrm{c}}\end{bmatrix}}_{\vec{u}_{\mathrm{acc}}} \tag{15b}$$

where the prefixes Δ in (15) are disregarded for simplification.

Accordingly, the state-space model of overall ACC can be established as

$$\dot{\vec{x}}_{\mathrm{acc}}=A_{\mathrm{acc}}\vec{x}_{\mathrm{acc}}+B_{\mathrm{acc}}\vec{u}_{\mathrm{acc}} \tag{16a}$$

$$\vec{y}_{\mathrm{acc}}=C_{\mathrm{acc}}\vec{x}_{\mathrm{acc}}+D_{\mathrm{acc}}\vec{u}_{\mathrm{acc}} \tag{16b}$$

where A_{acc}, B_{acc}, C_{acc}, D_{acc} are the matrices of the state-space model of ACC, which can be formulated according to the rule defined in (6), using matrices F_{acc}, H_{acc}, J_{acc}, K_{acc} in (12) and L_{acc1}, L_{acc2}, L_{acc3}, L_{acc4} in (15).

B. Phase-Locked Loop

Two dq-frames are defined in this paper to include the dynamics of the PLL [8]. One is the grid dq-frame that defined by the phase angle of fundamental positive-sequence PCC voltage **v**, denoted as θ_1. The other is the converter dq-frame, which is defined by the phase angle obtained from conventional SRF-PLL, denoted as θ. The input and output variables of the state-space model in the converter dq-frame will be denoted with the superscript c.

The control scheme of the synchronous rotating frame (SRF) PLL is shown in Fig. 5, where v_α, v_β are the PCC voltages in the $\alpha\beta$-frame; $G_{\mathrm{pll}}(s)$ is the PLL controller.

According to Fig. 5, the open-loop transfer function between the input q-axis voltage perturbation $\Delta v_{\mathrm{q}}^{\mathrm{c}}$ and the output synchronization angle variation $\Delta\theta$ is given by:

$$\Delta\theta = \underbrace{\left(k_{\mathrm{pp}} + k_{\mathrm{ip}}\frac{1}{s}\right)}_{G_{\mathrm{pll}}(s)} \cdot \frac{1}{s} \cdot \Delta v_{\mathrm{q}}^{\mathrm{c}} \tag{17}$$

In the time domain, (17) can be expressed by two differential equations:

$$\frac{d\phi_{\mathrm{q}}}{dt} = \Delta v_{\mathrm{q}}^{\mathrm{c}} \tag{18a}$$

$$\frac{d\Delta\theta}{dt} = k_{\mathrm{pp}}\Delta v_{\mathrm{q}}^{\mathrm{c}} + k_{\mathrm{ip}}\phi_{\mathrm{q}} \tag{18b}$$

Therefore, the state-space model for the SRF-PLL can be given by:

$$\underbrace{\begin{bmatrix} \dot{\phi}_{\mathrm{q}} \\ \Delta\dot{\theta} \end{bmatrix}}_{\dot{\vec{x}}_{\mathrm{pll}}} = \underbrace{\begin{bmatrix} 0 & 0 \\ k_{\mathrm{ip}} & 0 \end{bmatrix}}_{F_{\mathrm{pll}}} \underbrace{\begin{bmatrix} \phi_{\mathrm{q}} \\ \Delta\theta \end{bmatrix}}_{\vec{x}_{\mathrm{pll}}} + \underbrace{\begin{bmatrix} 1 \\ k_{\mathrm{pp}} \end{bmatrix}}_{H_{\mathrm{pll}}} \underbrace{\begin{bmatrix} \Delta v_{\mathrm{q}}^{\mathrm{c}} \end{bmatrix}}_{\vec{a}_{\mathrm{pll}}} \tag{19a}$$

$$\underbrace{\begin{bmatrix} \Delta\theta \end{bmatrix}}_{\vec{b}_{\mathrm{pll}}} = \underbrace{\begin{bmatrix} 0 & 1 \end{bmatrix}}_{J_{\mathrm{pll}}} \underbrace{\begin{bmatrix} \phi_{\mathrm{q}} \\ \Delta\theta \end{bmatrix}}_{\vec{x}_{\mathrm{pll}}} + \underbrace{\begin{bmatrix} 0 \end{bmatrix}}_{K_{\mathrm{pll}}} \underbrace{\begin{bmatrix} \Delta v_{\mathrm{q}}^{\mathrm{c}} \end{bmatrix}}_{\vec{a}_{\mathrm{pll}}} \tag{19b}$$

C. Dc-Link Voltage Control

The block scheme of the dc-link voltage control is shown in Fig. 6. To avoid the operating-point-dependent control dynamics, the voltage-square control scheme is employed [31], i.e., using the error $\left(v_{\mathrm{dc\_ref}}^2 - v_{\mathrm{dc}}^2\right)/2$ to calculate the power reference P_{ref}, and then generate the d-axis current reference.

The active power reference in the frequency domain can be given by:

$$P_{\mathrm{ref}} = \underbrace{\left(k_{\mathrm{pd}} + \frac{k_{\mathrm{id}}}{s}\right)}_{G_{\mathrm{dc}}(s)} \frac{v_{\mathrm{dc\_ref}}^2 - v_{\mathrm{dc}}^2}{2} \tag{20}$$

Therefore, the small-signal variation of the active power reference ΔP_{ref} resulted from dc-link voltage perturbation Δv_{dc} can be expressed by

$$\Delta P_{\mathrm{ref}} = -G_{\mathrm{dc}}(s)V_{\mathrm{dc0}}\Delta v_{\mathrm{dc}} \tag{21}$$

where V_{dc0} is the rated dc-link voltage.

The d-axis current reference is generated by:

$$i_{\mathrm{d\_ref}} = -\frac{P_{\mathrm{ref}}}{V_1} \Rightarrow \Delta i_{\mathrm{d\_ref}} = -\frac{\Delta P_{\mathrm{ref}}}{V_1} = \frac{G_{\mathrm{dc}}(s)V_{\mathrm{dc0}}}{V_1}\Delta v_{\mathrm{dc}} \tag{22}$$

where V_1 is the rated voltage at the PCC point.

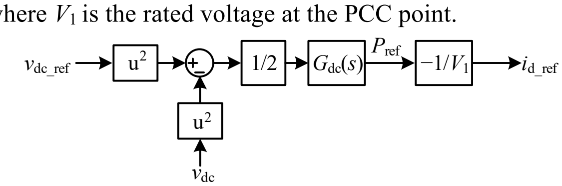

Fig. 6. Block diagram of dc-link voltage control (DVC)

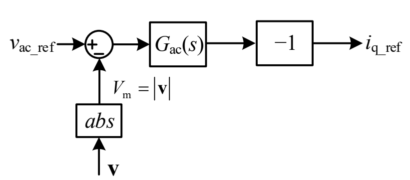

Fig. 7. Block diagram of the ac voltage magnitude control (AVC)

In the time domain, (22) can be expressed by

$$\frac{d\gamma_{\mathrm{dc}}}{dt} = \Delta v_{\mathrm{dc}} \tag{23a}$$

$$\Delta i_{\mathrm{d\_ref}} = \frac{k_{\mathrm{pd}}V_{\mathrm{dc0}}}{V_1}\Delta v_{\mathrm{dc}} + \frac{k_{\mathrm{id}}V_{\mathrm{dc0}}}{V_1}\gamma_{\mathrm{dc}} \tag{23b}$$

According (23), the state-space model of the DVC can be derived as:

$$\underbrace{\begin{bmatrix} \dot{\gamma}_{\mathrm{dc}} \end{bmatrix}}_{\dot{\vec{x}}_{\mathrm{dvc}}} = \underbrace{\begin{bmatrix} 0 \end{bmatrix}}_{F_{\mathrm{dvc}}} \underbrace{\begin{bmatrix} \gamma_{\mathrm{dc}} \end{bmatrix}}_{\vec{x}_{\mathrm{dvc}}} + \underbrace{\begin{bmatrix} 1 \end{bmatrix}}_{H_{\mathrm{dvc}}} \underbrace{\begin{bmatrix} \Delta v_{\mathrm{dc}} \end{bmatrix}}_{\vec{a}_{\mathrm{dvc}}} \tag{24a}$$

$$\underbrace{\begin{bmatrix} \Delta i_{\mathrm{d\_ref}} \end{bmatrix}}_{\vec{b}_{\mathrm{dvc}}} = \underbrace{\begin{bmatrix} \dfrac{k_{\mathrm{id}}V_{\mathrm{dc0}}}{V_1} \end{bmatrix}}_{J_{\mathrm{dvc}}} \underbrace{\begin{bmatrix} \gamma_{\mathrm{dc}} \end{bmatrix}}_{\vec{x}_{\mathrm{dvc}}} + \underbrace{\begin{bmatrix} \dfrac{k_{\mathrm{pd}}V_{\mathrm{dc0}}}{V_1} \end{bmatrix}}_{K_{\mathrm{dvc}}} \underbrace{\begin{bmatrix} \Delta v_{\mathrm{dc}} \end{bmatrix}}_{\vec{a}_{\mathrm{dvc}}} \tag{24b}$$

D. AC Voltage Magnitude Control

The block diagram of the ac voltage magnitude control is shown in Fig. 7.

Assuming that the AC voltage is regulated using the droop control method, then the expression of the q-axis current reference can be given by:

$$i_{\mathrm{q\_ref}} = -\underbrace{\frac{k_{\mathrm{pa}}\omega_{\mathrm{ac}}}{s + \omega_{\mathrm{ac}}}}_{G_{\mathrm{ac}}(s)}\left(v_{\mathrm{ac\_ref}} - V_{\mathrm{m}}\right) \tag{25}$$

where $V_{\mathrm{m}} = |\mathbf{v}| = \sqrt{v_{\mathrm{d}}^2 + v_{\mathrm{q}}^2}$. The small-signal variation of voltage magnitude ΔV_{m} resulted from the Δv_{d} and Δv_{q} can be derived as:

$$\left(V_{\mathrm{m1}} + \Delta V_{\mathrm{m}}\right)^2 = \left(V_1 + \Delta v_{\mathrm{d}}\right)^2 + \Delta v_{\mathrm{q}}^2 \Rightarrow \Delta V_{\mathrm{m}} \approx \Delta v_{\mathrm{d}} \tag{26}$$

According (25) and (26), it can be obtained that

$$\Delta i_{\mathrm{q\_ref}} = \frac{k_{\mathrm{pa}}\omega_{\mathrm{ac}}}{s + \omega_{\mathrm{ac}}}\Delta v_{\mathrm{d}} \tag{27}$$

In the time domain, (27) can be expressed by

$$\frac{dx_{\mathrm{ac}}}{dt} = -\omega_{\mathrm{ac}}x_{\mathrm{ac}} + k_{\mathrm{pa}}\omega_{\mathrm{ac}}\Delta v_{\mathrm{d}} \tag{28a}$$

$$x_{\mathrm{ac}} = \Delta i_{\mathrm{q\_ref}} \tag{28b}$$

Then the state-space model of AVC can be derived as:

$$\underbrace{\begin{bmatrix} \dot{x}_{\mathrm{ac}} \end{bmatrix}}_{\dot{\vec{x}}_{\mathrm{avc}}} = \underbrace{\begin{bmatrix} -\omega_{\mathrm{ac}} \end{bmatrix}}_{F_{\mathrm{avc}}} \underbrace{\begin{bmatrix} x_{\mathrm{ac}} \end{bmatrix}}_{\vec{x}_{\mathrm{avc}}} + \underbrace{\begin{bmatrix} k_{\mathrm{pa}}\omega_{\mathrm{ac}} \end{bmatrix}}_{H_{\mathrm{avc}}} \underbrace{\begin{bmatrix} \Delta v_{\mathrm{d}} \end{bmatrix}}_{\vec{a}_{\mathrm{avc}}} \tag{29a}$$

$$\underbrace{\begin{bmatrix} \Delta i_{\mathrm{qref}} \end{bmatrix}}_{\vec{b}_{\mathrm{avc}}} = \underbrace{\begin{bmatrix} 1 \end{bmatrix}}_{J_{\mathrm{avc}}} \underbrace{\begin{bmatrix} x_{\mathrm{ac}} \end{bmatrix}}_{\vec{x}_{\mathrm{avc}}} + \underbrace{\begin{bmatrix} 0 \end{bmatrix}}_{K_{\mathrm{avc}}} \underbrace{\begin{bmatrix} \Delta v_{\mathrm{d}} \end{bmatrix}}_{\vec{a}_{\mathrm{avc}}} \tag{29b}$$

IV. Implicit Sub-State-Space Models and Interconnections

The major challenge of CCM-based modeling in the converter-level lies in the representation of the implicit sub-state-space modes and implicit connections caused by the control couplings. The implicit connections between ACC and PLL can be established by linearizing the dq transformations. Moreover, the implicit connections and sub-state-space models between DVC control loop and voltages and currents at PCC can be obtained according to the active power balance principle.

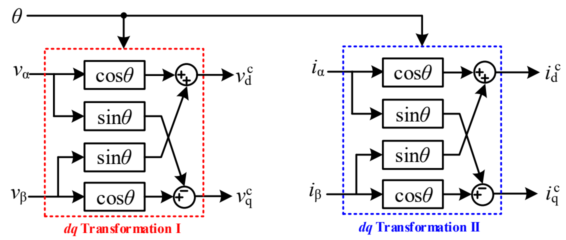

Fig. 8. Block diagram of *dq* transformations

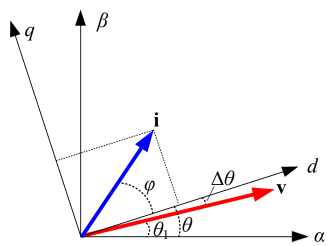

Fig. 9. Relationships of different phase angles

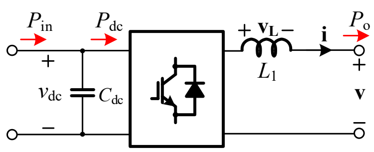

Fig. 10. Active power flow of VSC

A. *Dq-Transformation* I

As shown in Fig. 8, the inputs of *dq*-transformation I are PCC voltages in the stationary frame, i.e., v_α and v_β, and the synchronization angle θ obtained from the PLL; the outputs are PCC voltages in the converter *dq*-frame v_d^c, v_q^c. The input and output voltages can be represented in the complex space vector form, i.e.,

$$\mathbf{v}^s = v_\alpha + jv_\beta \quad \mathbf{v}^c = v_d^c + jv_q^c \tag{30}$$

The relationship between the PCC voltage vector $\mathbf{v}^s$ and converter *dq*-frame defined by synchronization angle θ is shown in Fig. 9. Accordingly, the *dq*-transformation can be expressed as

$$\mathbf{v}^c = \mathbf{v}^s \cdot e^{-j\theta} \tag{31}$$

Assuming that both inputs, including PCC voltages and synchronization angle, contain the small-signal perturbations, the PCC voltage in the stationary *αβ*-frame can be expressed as:

$$\mathbf{v}^s = \left(\mathbf{V}_1 + \mathbf{\Delta v}\right)e^{j\theta_1} \tag{32}$$

where $\mathbf{V}_1 = V_1 + j0$ is the steady-state PCC voltage vector in the grid *dq*-frame, and $\mathbf{\Delta v} = \Delta v_d + j\Delta v_q$ is the corresponding small-signal perturbation.

Similarly, the PLL output synchronization angle with the small-signal perturbation can be expressed by

$$\theta = \theta_1 + \Delta\theta \tag{33}$$

Substituting (33) and (32) into (31), yields

$$\begin{aligned}\mathbf{v}^c &= \mathbf{v}^s \cdot e^{-j\theta} = (V_1 + \mathbf{\Delta v})e^{j\theta_1}e^{-j(\theta_1+\Delta\theta)} \\ &= (V_1 + \mathbf{\Delta v})e^{-j\Delta\theta}\end{aligned} \tag{34}$$

Considering the small-signal perturbation $\Delta\theta$, and applying the first-order Taylor expansion, (34) can be approximated as:

$$\begin{aligned}\mathbf{v}^c &\approx (V_1 + \mathbf{\Delta v})(1 - j\Delta\theta) \\ &= \underbrace{V_1}_{\mathbf{V}_1^c} + \underbrace{\mathbf{\Delta v} - jV_1\mathbf{\Delta\theta} - j\mathbf{\Delta v}\Delta\theta}_{\mathbf{\Delta v}^c}\end{aligned} \tag{35}$$

By neglecting the second-order small-signal variation term $\mathbf{\Delta v}\Delta\theta$, the small-signal variation of PCC voltage in the converter *dq*-frame $\mathbf{\Delta v}^c$ can be obtained as

$$\mathbf{\Delta v}^c \approx \mathbf{\Delta v} - jV_1\Delta\theta = \Delta v_d^c + j\Delta v_q^c \tag{36}$$

Therefore, the relationship between the PCC voltages in converter *dq*-frame and grid *dq*-frame can be given by

$$\Delta v_d^c = \Delta v_d \tag{37a}$$

$$\Delta v_q^c = \Delta v_q - V_1\Delta\theta \tag{37b}$$

B. *Dq-Transformation* II

As shown in Fig. 8, the inputs of *dq*-transformation I are the PCC currents in the stationary frame, i.e., i_α and i_β, and the synchronization angle θ obtained from PLL; the outputs are the PCC currents in the converter *dq*-frame i_d^c, i_q^c. The input and output currents can be represented in the complex space vector form, i.e.,

$$\mathbf{i}^s = i_\alpha + ji_\beta \quad \mathbf{i}^c = i_d^c + ji_q^c \tag{38}$$

The relationship between the PCC current vector $\mathbf{i}^s$ and converter *dq*-frame defined by synchronization angle θ is shown in Fig. 9. Accordingly, the *dq*-transformation can be expressed as

$$\mathbf{i}^c = \mathbf{i}^s \cdot e^{-j\theta} \tag{39}$$

Assuming that PCC current vector contains the small-signal perturbations, i.e.,

$$\mathbf{i}^s = \left(\mathbf{i}_1 + \mathbf{\Delta i}\right)e^{j\theta_1} \tag{40}$$

where $\mathbf{I}_1 = I_{d1} + jI_{q1}$ is the steady-state PCC current vector in the grid *dq*-frame and thereby $\varphi = \arctan(I_{q1}/I_{d1})$; $\mathbf{\Delta i} = \Delta i_d + j\Delta i_q$ is the corresponding small-signal perturbation.

Substituting (33) and (40) into (39), yields

$$\begin{aligned}\mathbf{i}^c &= \mathbf{i}^s e^{-j\theta} = (\mathbf{I}_1 + \mathbf{\Delta i})e^{-j\Delta\theta} \approx \left(\mathbf{I}_1 + \mathbf{\Delta i}\right)\left(1 - j\Delta\theta\right) \\ &= \mathbf{I}_1 + \underbrace{\mathbf{\Delta i} - j\mathbf{I}_1\Delta\theta - j\mathbf{\Delta i}\Delta\theta}_{\mathbf{\Delta i}^c}\end{aligned} \tag{41}$$

By neglecting the second-order small-signal variation term $\mathbf{\Delta i}\Delta\theta$, it can be obtained that

$$\mathbf{\Delta i}^c \approx \mathbf{\Delta i} - j\mathbf{I}_1\Delta\theta = \Delta i_d^c + j\Delta i_q^c \tag{42}$$

Therefore, the relationship between the PCC currents in grid *dq*-frame and converter *dq*-frame can be given by

$$\Delta i_d = \Delta i_d^c - I_{q1}\Delta\theta \tag{43a}$$

$$\Delta i_q = \Delta i_q^c + I_{d1}\Delta\theta \tag{43b}$$

C. *Active Power Balance*

As shown in Fig. 10, the dynamic equation for the dc-link capacitor can be given by

$$\frac{1}{2}C_{dc}\frac{d\left(v_{dc}^2\right)}{dt} = P_{in} - P_{dc} \tag{44}$$

Applying the small-signal perturbation, yields

$$C_{dc}V_{dc0}\frac{d\Delta v_{dc}}{dt}=\Delta P_{in}-\Delta P_{dc} \tag{45}$$

Assuming that input power fluctuation is negligible, i.e., $\Delta P_{in}\approx 0$ and the power switches are ideal with no loss, the input active power injected into the dc side of VSC is equal to the output active power at the ac side, i.e., $\Delta P_{dc}\approx dE_L/dt+\Delta P_o$, where E_L is the energy storage in the inductor L_1.

The energy stored in the inductor L_1 can be given by

$$E_L=\frac{1}{2}L_1\mathbf{i}^2=\frac{1}{2}L_1\left(i_d^2+i_q^2\right) \tag{46}$$

Applying the small-signal perturbation, yields

$$\frac{dE_L}{dt}=L_1\left(I_{d1}\cdot\frac{d\Delta i_d}{dt}+I_{q1}\cdot\frac{d\Delta i_q}{dt}\right) \tag{47}$$

The output instantaneous complex power at the PCC is expressed by

$$\begin{aligned}\mathbf{S_o}&=\mathbf{vi}^*\approx V_1\mathbf{i}_1^*+V_1\cdot\Delta\mathbf{i}^*+\Delta\mathbf{v}\cdot\mathbf{i}_1^*\\&=\underbrace{V_1I_{d1}}_{P_{o1}}+\underbrace{I_{d1}\Delta v_d+I_{q1}\Delta ve+V_1\Delta i_d}_{\Delta P_o}\\&\quad+j\underbrace{\left(-V_1I_{q1}\right)}_{Q_{o1}}+j\underbrace{\left(I_{d1}\Delta v_q-I_{q1}\Delta v_d-V_1\Delta i_q\right)}_{\Delta Q_o}\\&\Rightarrow\Delta P_o=I_{d1}\Delta v_d+I_{q1}\Delta v_q+V_1\Delta i_d\end{aligned} \tag{48}$$

Considering $\Delta P_{dc}\approx dE_L/dt+\Delta P_o$, and substituting (47) and (48) into (45), yields

$$\begin{aligned}&C_{dc}V_{dc0}\frac{d\Delta v_{dc}}{dt}=\\&-\left(L_1I_{d1}\cdot\frac{d\Delta i_d}{dt}+L_1I_{q1}\cdot\frac{d\Delta i_q}{dt}+I_{d1}\Delta v_d+I_{q1}\Delta v_q+V_1\Delta i_d\right)\end{aligned} \tag{49}$$

which can be further rewritten as

$$\frac{dx_{dc}}{dt}=\frac{I_{d1}}{C_{dc}V_{dc0}}\Delta v_d+\frac{I_{q1}}{C_{dc}V_{dc0}}\Delta v_q+\frac{V_1}{C_{dc}V_{dc0}}\Delta i_d \tag{50a}$$

$$\Delta v_{dc}=-\left(\frac{L_1I_{d1}\Delta i_d+L_1I_{q1}\Delta i_q}{C_{dc}V_{dc0}}+x_{dc}\right) \tag{50b}$$

Consequently, an additional state-space model of active power balance can be established to represent the implicit connections between the dc-link voltage dynamics and the PCC voltages and currents, which is expressed as

$$\underbrace{\left[\dot{x}_{dc}\right]}_{\dot{\vec{x}}_{apb}}=\underbrace{\left[0\right]}_{F_{apb}}\underbrace{\left[x_{dc}\right]}_{\vec{x}_{apb}}+\underbrace{\begin{bmatrix}\frac{I_{d1}}{C_{dc}V_{dc0}} & \frac{I_{q1}}{C_{dc}V_{dc0}} & \frac{V_1}{C_{dc}V_{dc0}} & 0\end{bmatrix}}_{H_{apb}}\underbrace{\begin{bmatrix}\Delta v_d\\\Delta v_q\\\Delta i_d\\\Delta i_q\end{bmatrix}}_{\vec{a}_{apb}} \tag{51a}$$

$$\underbrace{\left[\Delta v_{dc}\right]}_{\vec{b}_{apb}}=\underbrace{\left[-1\right]}_{J_{apb}}\underbrace{\left[x_{dc}\right]}_{\vec{x}_{apb}}+\underbrace{\begin{bmatrix}0 & 0 & -\frac{L_1I_{d1}}{C_{dc}V_{dc0}} & -\frac{L_1I_{q1}}{C_{dc}V_{dc0}}\end{bmatrix}}_{K_{apb}}\underbrace{\begin{bmatrix}\Delta v_d\\\Delta v_q\\\Delta i_d\\\Delta i_q\end{bmatrix}}_{\vec{a}_{apb}} \tag{51b}$$

According to physical connections in Fig. 1 and implicit connections in (37), (43), (51), the overall connections among different control loops can be depicted by Fig. 11, where the prefixes Δ are disregarded for simplification.

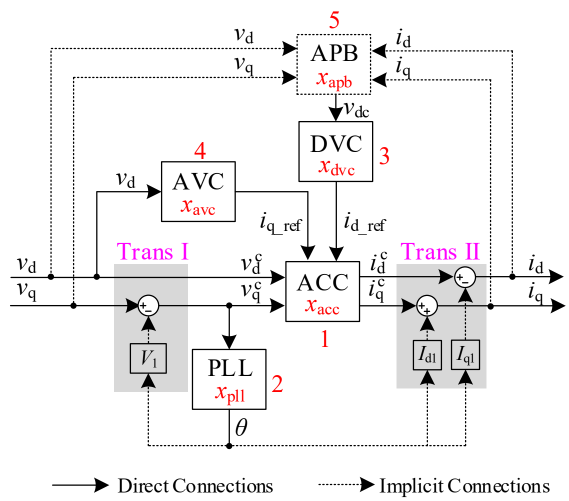

Fig. 11. Interconnection relationships among different control loops

V. System State-Space Model in the DQ-Frame

A. State-space Model of VSC

Considering the state-space models of ACC, PLL, DVC, AVC, and APB, the composite system model of VSC can be given by:

$$\underbrace{\begin{bmatrix}\dot{\vec{x}}_{acc}\\\dot{\vec{x}}_{pll}\\\dot{\vec{x}}_{dvc}\\\dot{\vec{x}}_{avc}\\\dot{\vec{x}}_{apb}\end{bmatrix}}_{\dot{\vec{x}}_{vsc}}=F_{vsc}\cdot\underbrace{\begin{bmatrix}\vec{x}_{acc}\\\vec{x}_{pll}\\\vec{x}_{dvc}\\\vec{x}_{avc}\\\vec{x}_{apb}\end{bmatrix}}_{\vec{x}_{vsc}}+H_{vsc}\cdot\underbrace{\begin{bmatrix}\vec{u}_{acc}\\\vec{a}_{pll}\\\vec{a}_{dvc}\\\vec{a}_{avc}\\\vec{a}_{apb}\end{bmatrix}}_{\vec{a}_{vsc}} \tag{52a}$$

$$\underbrace{\begin{bmatrix}\vec{y}_{acc}\\\vec{b}_{pll}\\\vec{b}_{dvc}\\\vec{b}_{avc}\\\vec{b}_{apb}\end{bmatrix}}_{\vec{b}_{vsc}}=J_{vsc}\cdot\underbrace{\begin{bmatrix}\vec{x}_{acc}\\\vec{x}_{pll}\\\vec{x}_{dvc}\\\vec{x}_{avc}\\\vec{x}_{apb}\end{bmatrix}}_{\vec{x}_{vsc}}+K_{vsc}\cdot\underbrace{\begin{bmatrix}\vec{u}_{acc}\\\vec{a}_{pll}\\\vec{a}_{dvc}\\\vec{a}_{avc}\\\vec{a}_{apb}\end{bmatrix}}_{\vec{a}_{vsc}} \tag{52b}$$

where F_{vsc}=diag(A_{acc}, F_{pll}, F_{dvc}, F_{avc}, F_{apb}), H_{vsc}=diag(B_{acc}, H_{pll}, H_{dvc}, H_{avc}, H_{apb}), J_{vsc}=diag(C_{acc}, J_{pll}, J_{dvc}, J_{avc}, J_{apb}), K_{vsc}=diag(D_{acc}, K_{pll}, K_{dvc}, K_{avc}, K_{apb}), with the matrices A_{acc}, B_{acc}, C_{acc}, D_{acc} defined in (16), the matrices F_{pll}, H_{pll}, J_{pll}, K_{pll} defined in (19), the matrices F_{dvc}, H_{dvc}, J_{dvc}, K_{dvc} defined in (24), the matrices F_{avc}, H_{avc}, J_{avc}, K_{avc} defined in (29), the matrices F_{apb}, H_{apb}, J_{apb}, K_{apb} defined in (51).

According to Fig. 11, the input vector u_{vsc} and output vector y_{vsc} of overall VSC are expressed as

$$\vec{u}_{vsc}=\begin{bmatrix}v_d\\v_q\end{bmatrix}\qquad\vec{y}_{vsc}=\begin{bmatrix}i_d\\i_q\end{bmatrix} \tag{53}$$

The interconnection relationship can be described as:

$$
\begin{array}{c}\text{ACC}\\ \\ \\ \\ \text{PLL}\\ \text{DVC}\\ \text{AVC}\\ \\ \text{APB}\\ \\ \\ \end{array}
\underbrace{\begin{bmatrix} i_{\mathrm{d\_ref}} \\ i_{\mathrm{q\_ref}} \\ v_{\mathrm{d}}^{\mathrm{c}} \\ v_{\mathrm{q}}^{\mathrm{c}} \\ v_{\mathrm{q}}^{\mathrm{c}} \\ v_{\mathrm{dc}} \\ v_{\mathrm{d}} \\ v_{\mathrm{d}} \\ v_{\mathrm{q}} \\ i_{\mathrm{d}} \\ i_{\mathrm{q}} \end{bmatrix}}_{\vec{a}_{\mathrm{vsc}}}
=
\underbrace{\begin{bmatrix}
0 & 0 & 0 & 1 & 0 & 0 \\
0 & 0 & 0 & 0 & 1 & 0 \\
0 & 0 & 0 & 0 & 0 & 0 \\
0 & 0 & -V_1 & 0 & 0 & 0 \\
0 & 0 & -V_1 & 0 & 0 & 0 \\
0 & 0 & 0 & 0 & 0 & 1 \\
0 & 0 & 0 & 0 & 0 & 0 \\
0 & 0 & 0 & 0 & 0 & 0 \\
0 & 0 & 0 & 0 & 0 & 0 \\
1 & 0 & -I_{\mathrm{q1}} & 0 & 0 & 0 \\
0 & 1 & I_{\mathrm{d1}} & 0 & 0 & 0
\end{bmatrix}}_{L_{\mathrm{vsc1}}}
\underbrace{\begin{bmatrix} i_{\mathrm{d}}^{\mathrm{c}} \\ i_{\mathrm{q}}^{\mathrm{c}} \\ \theta \\ i_{\mathrm{d\_ref}} \\ i_{\mathrm{q\_ref}} \\ v_{\mathrm{dc}} \end{bmatrix}}_{\vec{b}_{\mathrm{vsc}}}
+
\underbrace{\begin{bmatrix}
0 & 0 \\ 0 & 0 \\ 1 & 0 \\ 0 & 1 \\ 0 & 1 \\ 0 & 0 \\ 1 & 0 \\ 1 & 0 \\ 0 & 1 \\ 0 & 0 \\ 0 & 0
\end{bmatrix}}_{L_{\mathrm{vsc2}}}
\underbrace{\begin{bmatrix} v_{\mathrm{d}} \\ v_{\mathrm{q}} \end{bmatrix}}_{\vec{u}_{\mathrm{vsc}}}
\tag{54a}
$$

$$
\underbrace{\begin{bmatrix} i_{\mathrm{d}} \\ i_{\mathrm{q}} \end{bmatrix}}_{\vec{y}_{\mathrm{vsc}}}
=
\underbrace{\begin{bmatrix}
1 & 0 & -I_{\mathrm{q1}} & 0 & 0 & 0 \\
0 & 1 & I_{\mathrm{d1}} & 0 & 0 & 0
\end{bmatrix}}_{L_{\mathrm{vsc3}}}
\underbrace{\begin{bmatrix} i_{\mathrm{d}}^{\mathrm{c}} \\ i_{\mathrm{q}}^{\mathrm{c}} \\ \theta \\ i_{\mathrm{d\_ref}} \\ i_{\mathrm{q\_ref}} \\ v_{\mathrm{dc}} \end{bmatrix}}_{\vec{b}_{\mathrm{vsc}}}
+
\underbrace{\begin{bmatrix} 0 & 0 \\ 0 & 0 \end{bmatrix}}_{L_{\mathrm{vsc4}}}
\underbrace{\begin{bmatrix} v_{\mathrm{d}} \\ v_{\mathrm{q}} \end{bmatrix}}_{\vec{u}_{\mathrm{vsc}}}
\tag{54b}
$$

Therefore the state-space model of VSC can be derived as

$$\dot{\vec{x}}_{\mathrm{vsc}} = A_{\mathrm{vsc}}\vec{x}_{\mathrm{vsc}} + B_{\mathrm{vsc}}\vec{u}_{\mathrm{vsc}} \tag{55a}$$

$$\vec{y}_{\mathrm{vsc}} = C_{\mathrm{vsc}}\vec{x}_{\mathrm{vsc}} + D_{\mathrm{vsc}}\vec{u}_{\mathrm{vsc}} \tag{55b}$$

where A_{vsc}, B_{vsc}, C_{vsc}, D_{vsc} are the matrices of the state-space model of ACC, which can be formulated according to the rule defined in (6), using matrices F_{vsc}, H_{vsc}, J_{vsc}, K_{vsc} in (52) and L_{vsc1}, L_{vsc2}, L_{vsc3}, L_{vsc4} in (54).

B. State-space Model of the Grid-Side Impedance

As for the equivalent grid impedance shown in Fig.1, its dynamic equations can be derived as:

$$C_{\mathrm{g}}\left(\frac{dv_{\mathrm{Cgd}}}{dt} - \omega_1 v_{\mathrm{Cgq}}\right) = i_{\mathrm{d}} - i_{\mathrm{Lgd}} \tag{56a}$$

$$L_{\mathrm{g}}\left(\frac{di_{\mathrm{Lgd}}}{dt} - \omega_1 i_{\mathrm{Lgq}}\right) + R_{\mathrm{Lg}} i_{\mathrm{Lgd}} = v_{\mathrm{Cgd}} + R_{\mathrm{Cg}}\left(i_{\mathrm{d}} - i_{\mathrm{Lgd}}\right) \tag{56b}$$

$$C_{\mathrm{g}}\left(\frac{dv_{\mathrm{Cgq}}}{dt} + \omega_1 v_{\mathrm{Cgd}}\right) = i_{\mathrm{q}} - i_{\mathrm{Lgq}} \tag{56c}$$

$$L_{\mathrm{g}}\left(\frac{di_{\mathrm{Lgq}}}{dt} + \omega_1 i_{\mathrm{Lgd}}\right) + R_{\mathrm{Lg}} i_{\mathrm{Lgq}} = v_{\mathrm{Cgq}} + R_{\mathrm{Cg}}\left(i_{\mathrm{q}} - i_{\mathrm{Lgq}}\right) \tag{56d}$$

where $v_{\mathrm{Cgd/q}}$ and $i_{\mathrm{Lgd/q}}$ are the grid capacitor voltage and grid inductor current, respectively; R_{Lg} and R_{Cg} are the ESRs of L_{g} and C_{g}, respectively.

According to (56), the state-space model of the grid impedance can be derived as

$$
\underbrace{\begin{bmatrix} \dot{v}_{\mathrm{Cgd}} \\ \dot{i}_{\mathrm{Lgd}} \\ \dot{v}_{\mathrm{Cgq}} \\ \dot{i}_{\mathrm{Lgq}} \end{bmatrix}}_{\dot{\vec{x}}_{\mathrm{g}}}
=
\underbrace{\begin{bmatrix}
0 & -\frac{1}{C_{\mathrm{g}}} & \omega_1 & 0 \\
\frac{1}{L_{\mathrm{g}}} & \frac{-R_{\mathrm{Lg}} - R_{\mathrm{Cg}}}{L_{\mathrm{g}}} & 0 & \omega_1 \\
-\omega_1 & 0 & 0 & -\frac{1}{C_{\mathrm{g}}} \\
0 & -\omega_1 & \frac{1}{L_{\mathrm{g}}} & \frac{-R_{\mathrm{Lg}} - R_{\mathrm{Cg}}}{L_{\mathrm{g}}}
\end{bmatrix}}_{F_{\mathrm{g}}}
\underbrace{\begin{bmatrix} v_{\mathrm{Cgd}} \\ i_{\mathrm{Lgd}} \\ v_{\mathrm{Cgq}} \\ i_{\mathrm{Lgq}} \end{bmatrix}}_{\vec{x}_{\mathrm{g}}}
+
\underbrace{\begin{bmatrix}
\frac{1}{C_{\mathrm{g}}} & 0 \\
\frac{R_{\mathrm{Cg}}}{L_{\mathrm{g}}} & 0 \\
0 & \frac{1}{C_{\mathrm{g}}} \\
0 & \frac{R_{\mathrm{Cg}}}{L_{\mathrm{g}}}
\end{bmatrix}}_{H_{\mathrm{g}}}
\underbrace{\begin{bmatrix} i_{\mathrm{d}} \\ i_{\mathrm{q}} \end{bmatrix}}_{\vec{a}_{\mathrm{g}}}
\tag{57a}
$$

$$
\underbrace{\begin{bmatrix} v_{\mathrm{d}} \\ v_{\mathrm{q}} \end{bmatrix}}_{\vec{b}_{\mathrm{g}}}
=
\underbrace{\begin{bmatrix} 1 & 0 & 0 & 0 \\ 0 & 0 & 1 & 0 \end{bmatrix}}_{J_{\mathrm{g}}}
\underbrace{\begin{bmatrix} v_{\mathrm{Cgd}} \\ i_{\mathrm{Lgd}} \\ v_{\mathrm{Cgq}} \\ i_{\mathrm{Lgq}} \end{bmatrix}}_{\vec{x}_{\mathrm{g}}}
+
\underbrace{\begin{bmatrix} 0 & 0 \\ 0 & 0 \end{bmatrix}}_{K_{\mathrm{g}}}
\underbrace{\begin{bmatrix} i_{\mathrm{d}} \\ i_{\mathrm{q}} \end{bmatrix}}_{\vec{a}_{\mathrm{g}}}
\tag{57b}
$$

C. State-space Model of Overall system

The block diagram of single VSC and grid impedance is given in Fig. 12. The composite system model of VSC and grid impedance can be given by:

$$
\underbrace{\begin{bmatrix} \dot{\vec{x}}_{\mathrm{vsc}} \\ \dot{\vec{x}}_{\mathrm{g}} \end{bmatrix}}_{\dot{\vec{x}}_{\mathrm{all}}}
=
\underbrace{\begin{bmatrix} A_{\mathrm{vsc}} & \\ & F_{\mathrm{g}} \end{bmatrix}}_{F_{\mathrm{all}}}
\underbrace{\begin{bmatrix} \vec{x}_{\mathrm{vsc}} \\ \vec{x}_{\mathrm{g}} \end{bmatrix}}_{\vec{x}_{\mathrm{all}}}
+
\underbrace{\begin{bmatrix} B_{\mathrm{vsc}} & \\ & H_{\mathrm{g}} \end{bmatrix}}_{H_{\mathrm{all}}}
\underbrace{\begin{bmatrix} \vec{u}_{\mathrm{vsc}} \\ \vec{a}_{\mathrm{g}} \end{bmatrix}}_{\vec{a}_{\mathrm{all}}}
\tag{58a}
$$

$$
\underbrace{\begin{bmatrix} \vec{y}_{\mathrm{vsc}} \\ \vec{b}_{\mathrm{g}} \end{bmatrix}}_{\vec{b}_{\mathrm{all}}}
=
\underbrace{\begin{bmatrix} C_{\mathrm{vsc}} & \\ & J_{\mathrm{g}} \end{bmatrix}}_{J_{\mathrm{all}}}
\underbrace{\begin{bmatrix} \vec{x}_{\mathrm{vsc}} \\ \vec{x}_{\mathrm{g}} \end{bmatrix}}_{\vec{x}_{\mathrm{all}}}
+
\underbrace{\begin{bmatrix} D_{\mathrm{vsc}} & \\ & K_{\mathrm{g}} \end{bmatrix}}_{K_{\mathrm{all}}}
\underbrace{\begin{bmatrix} \vec{u}_{\mathrm{vsc}} \\ \vec{a}_{\mathrm{g}} \end{bmatrix}}_{\vec{a}_{\mathrm{all}}}
\tag{58b}
$$

where the matrices A_{vsc}, B_{vsc}, C_{vsc}, D_{vsc} are defined in (55), the matrices F_{g}, H_{g}, J_{g}, K_{g} are defined in (57).

According to Fig. 12, the interconnections between the VSC and grid impedance can be explained by the following equations:

$$
\begin{array}{c}\text{VSC}\\ \\ Z_{\mathrm{g}}\\ \\ \end{array}
\underbrace{\begin{bmatrix} v_{\mathrm{d}} \\ v_{\mathrm{q}} \\ i_{\mathrm{d}} \\ i_{\mathrm{q}} \end{bmatrix}}_{\vec{a}_{\mathrm{all}}}
=
\underbrace{\begin{bmatrix} 0 & 0 & 1 & 0 \\ 0 & 0 & 0 & 1 \\ 1 & 0 & 0 & 0 \\ 0 & 1 & 0 & 0 \end{bmatrix}}_{L_{\mathrm{all1}}}
\underbrace{\begin{bmatrix} i_{\mathrm{d}} \\ i_{\mathrm{q}} \\ v_{\mathrm{d}} \\ v_{\mathrm{q}} \end{bmatrix}}_{\vec{b}_{\mathrm{all}}}
+
\underbrace{\begin{bmatrix} 0 \\ 0 \\ 0 \\ 0 \end{bmatrix}}_{L_{\mathrm{all2}}}
\underbrace{\begin{bmatrix} 0 \end{bmatrix}}_{\vec{u}_{\mathrm{all}}}
\tag{59a}
$$

$$
\underbrace{\begin{bmatrix} 0 \end{bmatrix}}_{\vec{y}_{\mathrm{all}}}
=
\underbrace{\begin{bmatrix} 0 & 0 & 0 & 0 \end{bmatrix}}_{L_{\mathrm{all3}}}
\underbrace{\begin{bmatrix} i_{\mathrm{d}} \\ i_{\mathrm{q}} \\ v_{\mathrm{d}} \\ v_{\mathrm{q}} \end{bmatrix}}_{\vec{b}_{\mathrm{all}}}
+
\underbrace{\begin{bmatrix} 0 \end{bmatrix}}_{L_{\mathrm{all4}}}
\underbrace{\begin{bmatrix} 0 \end{bmatrix}}_{\vec{u}_{\mathrm{all}}}
\tag{59b}
$$

Thus, the whole system state-space model can be obtained as

$$\dot{\vec{x}}_{\mathrm{all}} = A_{\mathrm{all}}\vec{x}_{\mathrm{all}} + B_{\mathrm{all}}\vec{u}_{\mathrm{all}} \tag{60a}$$

$$\vec{y}_{\mathrm{all}} = C_{\mathrm{all}}\vec{x}_{\mathrm{all}} + D_{\mathrm{all}}\vec{u}_{\mathrm{all}} \tag{60b}$$

where A_{all}, B_{all}, C_{all}, D_{all} are obtained using (58) and (59), expressed as

$$A_{\mathrm{all}} = F_{\mathrm{all}} + H_{\mathrm{all}} L_{\mathrm{all1}} \left(I - K_{\mathrm{all}} L_{\mathrm{all1}}\right)^{-1} J_{\mathrm{all}} \tag{61a}$$

$$B_{\mathrm{all}} = C_{\mathrm{all}} = D_{\mathrm{all}} = 0 \tag{61b}$$

and $\vec{x}_{\mathrm{all}}$ can be expended as (61c).

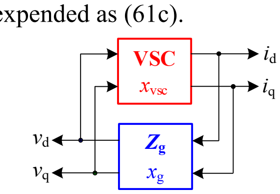

Fig. 12. Block diagram of VSC and grid impedance

$$\vec{x}_{\mathrm{all}} = [\gamma_{\mathrm{id}} \;\; \gamma_{\mathrm{iq}} \;\; x_{\mathrm{ff\_d}} \;\; x_{\mathrm{ff\_q}} \;\; x_{\mathrm{del\_1d}} \;\; x_{\mathrm{del\_2d}} \;\; x_{\mathrm{del\_3d}} \;\; x_{\mathrm{del\_1q}} \;\; x_{\mathrm{del\_2q}} \;\; x_{\mathrm{del\_3q}} \;\; i_{\mathrm{d}}^{\mathrm{c}} \;\; i_{\mathrm{q}}^{\mathrm{c}} \mid \phi_{\mathrm{q}} \;\; \theta \mid \gamma_{\mathrm{dc}} \mid x_{\mathrm{ac}} \mid x_{\mathrm{dc}} \mid v_{\mathrm{Cgd}} \;\; i_{\mathrm{Lgd}} \;\; v_{\mathrm{Cgq}} \;\; i_{\mathrm{Lgq}}]^{T} \tag{61c}$$

VI. Mathematical Relationship Between State-Space Models in Different Frames

In order to bridge the state-space models of VSC in the dq-frame and the $\alpha\beta$-frame, the relationships between the variables in the two frames have to be established.

Assumed that the state-space model of the subsystem or the whole system in the dq-frame is denoted by:

$$\dot{\vec{x}}_{\mathrm{dq}} = A_{\mathrm{dq}}\vec{x}_{\mathrm{dq}} + B_{\mathrm{dq}}\vec{u}_{\mathrm{dq}} \tag{62a}$$

$$\vec{y}_{\mathrm{dq}} = C_{\mathrm{dq}}\vec{x}_{\mathrm{dq}} + D_{\mathrm{dq}}\vec{u}_{\mathrm{dq}} \tag{62b}$$

which can represent the state-space models of components or the whole system.

The variables in the state vector $\vec{x}_{\mathrm{dq}}$, input vector $\vec{u}_{\mathrm{dq}}$, and the output vector $\vec{y}_{\mathrm{dq}}$ can be categorized into two types. One type is the variable that appeared in dq pairs, such as i_{d} and i_{q}. The other type is the variable does not have their d or q counterparts, such as v_{dc} and θ.

As for the dq pairs, taking x_{d} and x_{q} as the example, the complex space vector and its conjugation can be defined as

$$\mathbf{x_{dq}} = x_{\mathrm{d}} + jx_{\mathrm{q}} \tag{63a}$$

$$\mathbf{x^*_{dq}} = x_{\mathrm{d}} - jx_{\mathrm{q}} \tag{63b}$$

Then, the transformation between dq pairs and complex space vectors can be obtained as

$$\begin{bmatrix} x_{\mathrm{d}} \\ x_{\mathrm{q}} \end{bmatrix} = \frac{1}{2}\begin{bmatrix} 1 & 1 \\ -j & j \end{bmatrix} \cdot \begin{bmatrix} \mathbf{x_{dq}} \\ \mathbf{x^*_{dq}} \end{bmatrix} \tag{64}$$

As for the single variable, take x_{s} as an example, it can be treated as the real part of a virtual complex space vector $\tilde{\mathbf{x}}_{\mathbf{dq}}$ [32], which can be expressed by

$$\tilde{\mathbf{x}}_{\mathbf{dq}} = x_{\mathrm{s}} + jx_{\mathrm{v}} \tag{65}$$

where x_{v} is the virtual imaginary part. Since x_{v} is the virtual variable with no physical meaning, it can be set to zero for simplification and thereby $x_{\mathrm{s}} = \tilde{\mathbf{x}}_{\mathbf{dq}}$.

Consequently, the transformation rule from the real state vector $\vec{x}_{\mathrm{dq}}$ to the complex space state vector $\vec{\mathbf{X}}_{\mathbf{dq}}$ can be obtained as

$$\underbrace{\begin{bmatrix} \vdots \\ x_{\mathrm{d}} \\ x_{\mathrm{q}} \\ \vdots \\ x_{\mathrm{s}} \\ \vdots \end{bmatrix}}_{\vec{x}_{\mathrm{dq}}} = \frac{1}{2}\underbrace{\begin{bmatrix} \ddots & & & & \\ & 1 & 1 & & \\ & -j & j & & \\ & & & \ddots & & \\ & & & & 2 & \\ & & & & & \ddots \end{bmatrix}}_{T_{\mathrm{x}}} \cdot \underbrace{\begin{bmatrix} \vdots \\ \mathbf{x_{dq}} \\ \mathbf{x^*_{dq}} \\ \vdots \\ \tilde{\mathbf{x}}_{\mathbf{dq}} \\ \vdots \end{bmatrix}}_{\vec{\mathbf{X}}_{\mathbf{dq}}} \tag{66}$$

The state complex space vector $\vec{\mathbf{X}}_{\mathbf{dq}}$ in (66) can be further translated to the stationary frame, which can be expressed as

$$\underbrace{\begin{bmatrix} \vdots \\ \mathbf{x_{dq}} \\ \mathbf{x^*_{dq}} \\ \vdots \\ \tilde{\mathbf{x}}_{\mathbf{dq}} \\ \vdots \end{bmatrix}}_{\vec{\mathbf{X}}_{\mathbf{dq}}} = \begin{bmatrix} \vdots \\ \mathbf{x}_{\boldsymbol{\alpha\beta}}e^{-j\theta_1} \\ \mathbf{x}^*_{\boldsymbol{\alpha\beta}}e^{j\theta_1} \\ \vdots \\ \tilde{\mathbf{x}}_{\boldsymbol{\alpha\beta}}e^{-j\theta_1} \\ \vdots \end{bmatrix} = e^{-j\theta_1}\underbrace{\begin{bmatrix} \vdots \\ \mathbf{x}_{\boldsymbol{\alpha\beta}} \\ \mathbf{x}^*_{\boldsymbol{\alpha\beta}}e^{j2\theta_1} \\ \vdots \\ \tilde{\mathbf{x}}_{\boldsymbol{\alpha\beta}} \\ \vdots \end{bmatrix}}_{\vec{\mathbf{X}}_{\boldsymbol{\alpha\beta}}} \tag{67}$$

Substituting (67) into (66), yields

$$\vec{x}_{\mathrm{dq}} = T_{\mathrm{x}} \cdot \vec{\mathbf{X}}_{\mathbf{dq}} = T_{\mathrm{x}} \cdot e^{-j\theta_1} \cdot \vec{\mathbf{X}}_{\boldsymbol{\alpha\beta}} \tag{68}$$

Similar transformation rule can be derived for the input vector $\vec{u}_{\mathrm{dq}}$, and the output vector $\vec{y}_{\mathrm{dq}}$, which are defined as

$$\vec{u}_{\mathrm{dq}} = T_{\mathrm{u}} \cdot \vec{\mathbf{U}}_{\mathbf{dq}} = T_{\mathrm{u}} \cdot e^{-j\theta_1} \cdot \vec{\mathbf{U}}_{\boldsymbol{\alpha\beta}} \tag{69a}$$

$$\vec{y}_{\mathrm{dq}} = T_{\mathrm{y}} \cdot \vec{\mathbf{Y}}_{\mathbf{dq}} = T_{\mathrm{y}} \cdot e^{-j\theta_1} \cdot \vec{\mathbf{Y}}_{\boldsymbol{\alpha\beta}} \tag{69b}$$

Substituting (68) and (69) into (62), yields

$$\frac{d\left(T_{\mathrm{x}} \cdot e^{-j\theta_1} \cdot \vec{\mathbf{X}}_{\boldsymbol{\alpha\beta}}\right)}{dt} = A_{\mathrm{dq}} \cdot \left(T_{\mathrm{x}} \cdot e^{-j\theta_1} \cdot \vec{\mathbf{X}}_{\boldsymbol{\alpha\beta}}\right) + B_{\mathrm{dq}} \cdot \left(T_{\mathrm{u}} \cdot e^{-j\theta_1} \cdot \vec{\mathbf{U}}_{\boldsymbol{\alpha\beta}}\right) \tag{70a}$$

$$T_{\mathrm{y}} \cdot e^{-j\theta_1} \cdot \vec{\mathbf{Y}}_{\boldsymbol{\alpha\beta}} = C_{\mathrm{dq}} \cdot \left(T_{\mathrm{x}} \cdot e^{-j\theta_1} \cdot \vec{\mathbf{X}}_{\boldsymbol{\alpha\beta}}\right) + D_{\mathrm{dq}} \cdot \left(T_{\mathrm{u}} \cdot e^{-j\theta_1} \cdot \vec{\mathbf{U}}_{\boldsymbol{\alpha\beta}}\right) \tag{70b}$$

The derivative term in the left side of (70a) can be expended as:

$$\frac{d\left(T_{\mathrm{x}} \cdot e^{-j\theta_1} \cdot \vec{\mathbf{X}}_{\boldsymbol{\alpha\beta}}\right)}{dt} = T_{\mathrm{x}}e^{-j\theta_1} \cdot \frac{d\vec{\mathbf{X}}_{\boldsymbol{\alpha\beta}}}{dt} - j\omega_1 T_{\mathrm{x}} e^{-j\theta_1} \cdot \vec{\mathbf{X}}_{\boldsymbol{\alpha\beta}} \tag{71}$$

where $\omega_1 = d\theta_1/dt$. By substituting (71) into (70a), and eliminating $e^{-j\theta 1}$ from both sides of Eq. (70), the state-space model in stationary $\alpha\beta$-frame can be obtained as

$$\dot{\vec{\mathbf{X}}}_{\boldsymbol{\alpha\beta}} = T_{\mathrm{x}}^{-1}\left(A_{\mathrm{dq}} + j\omega_1 I\right)T_{\mathrm{x}} \cdot \vec{\mathbf{X}}_{\boldsymbol{\alpha\beta}} + T_{\mathrm{x}}^{-1}B_{\mathrm{dq}}T_{\mathrm{u}} \cdot \vec{\mathbf{U}}_{\boldsymbol{\alpha\beta}} \tag{72a}$$

$$\vec{\mathbf{Y}}_{\boldsymbol{\alpha\beta}} = T_{\mathrm{y}}^{-1}C_{\mathrm{dq}}T_{\mathrm{x}} \cdot \vec{\mathbf{X}}_{\boldsymbol{\alpha\beta}} + T_{\mathrm{y}}^{-1}D_{\mathrm{dq}}T_{\mathrm{u}} \cdot \vec{\mathbf{U}}_{\boldsymbol{\alpha\beta}} \tag{72b}$$

As a conclusion, the transformation between the matrices of the state-space model in the dq- and $\alpha\beta$-frames can be expressed by:

$$A_{\alpha\beta} = T_{\mathrm{x}}^{-1}\left(A_{\mathrm{dq}} + j\omega_1 I\right)T_{\mathrm{x}} \tag{73a}$$

$$B_{\alpha\beta} = T_{\mathrm{x}}^{-1}B_{\mathrm{dq}}T_{\mathrm{u}} \tag{73b}$$

$$C_{\alpha\beta} = T_{\mathrm{y}}^{-1}C_{\mathrm{dq}}T_{\mathrm{x}} \tag{73c}$$

$$D_{\alpha\beta} = T_{\mathrm{y}}^{-1}D_{\mathrm{dq}}T_{\mathrm{u}} \tag{73d}$$

VII. Modal Analysis Using Unified State-Space Model

The modal analysis is a common practice for the small-signal stability of power grids, which is mainly about how to interpret the dynamic modes of system by analyzing the eigenvalues, eigenvectors, participation factor and sensitivity of the state matrix in the state-space models. Since the modal analysis procedures are the same for the dq state matrix A_{dq} and $\alpha\beta$ state matrix $A_{\alpha\beta}$, therefore the notation $A_{\mathrm{dq}/\alpha\beta}$ is used to stand for either A_{dq} or $A_{\alpha\beta}$ for the following analysis.

The eigenvalues of state-matrix $A_{\mathrm{dq}/\alpha\beta}$ can be derived by:

$$\det\left(\lambda I - A_{\mathrm{dq}/\alpha\beta}\right) = 0 \tag{74}$$

Assuming that $A_{\mathrm{dq}/\alpha\beta}$ is n by n matrix, n eigenvalues can be obtained by solving (74).

Supposing that h^{th} eigenvalue of $A_{\mathrm{dq}/\alpha\beta}$, λ_h, is expressed by:

$$\lambda_h = \sigma_h + j\omega_h \tag{75}$$

Then corresponding frequency f_h and damping ratio ζ_h of h^{th} dynamic mode can be obtained as

$$f_h = \frac{\omega_h}{2\pi} \tag{76a}$$

$$\varsigma_h = -\frac{\sigma_h}{\sqrt{\sigma_h^2 + \omega_h^2}} \tag{76b}$$

The stability of the h^{th} dynamic mode can be assessed by the value of ζ_h: when ζ_h >0, the mode is stable; when ζ_h = 0, the mode is marginally stable; when ζ_h <0, the mode is unstable.

The right eigenvector $\mathbf{R}_h$ of λ_h is defined as

$$A_{\mathrm{dq/\alpha\beta}} \cdot \mathbf{R}_h = \lambda_h \cdot \mathbf{R}_h \tag{77}$$

which contains n elements, indicating the magnitudes and phase angles of n state variables of $x_{\mathrm{dq}}/\mathbf{X}_{\alpha\beta}$, respectively, in the h^{th} dynamic mode [33], i.e.,

$$\mathbf{R}_h = \begin{bmatrix} M_1 e^{\varphi_1} \\ \vdots \\ M_i e^{\varphi_i} \\ \vdots \\ M_n e^{\varphi_n} \end{bmatrix} \begin{matrix} \rightarrow \\ \\ \rightarrow \\ \\ \rightarrow \end{matrix} \begin{bmatrix} x_1 \\ \vdots \\ x_i \\ \vdots \\ x_n \end{bmatrix} = \vec{x}_{\mathrm{dq}} / \vec{\mathbf{X}}_{\alpha\beta} \tag{78}$$

To provide a good insight into the tuning the control parameters to damp the critical dynamic modes, the sensitivity of the damping ratio with respect to the specific control parameter can be also calculated. The damping ratio ζ_h with respect to the control parameter p can be obtained as

$$\frac{\partial \varsigma_h}{\partial p} \approx \frac{\varsigma_h(p_0 + \Delta p) - \varsigma_h(p_0)}{\Delta p} \tag{79}$$

where p_0 is the original control parameter, and Δp=5%~10% p_0 is the parameter perturbation.

It should be noted that since the elements of $A_{\alpha\beta}$ are complex numbers, the eigenvalues of complex matrix $A_{\alpha\beta}$ are not paired with their conjugations, which can directly reveal the coupled oscillation frequencies in the $\alpha\beta$ frame caused by the asymmetrical dynamics of the control system.

VIII. Experimental Verification

In order to verify the correctness of the unified modular state-space model and modal analysis, a down-scaled experimental setup is built in the lab, as shown in Fig. 13, where two converters are operated back-to-back. The converter 1# draws the constant magnitude of current at ac side, which can be treated as a constant power source given that both the power loss and ac voltage magnitude of converter 1# are constant. The converter 2# is the grid-connected VSC, which contains ACC, PLL, DVC and AVC control loops. All the control algorithms are implemented in the dSPACE 1007. The capacitor C_g and inductor L_g are connected with grid simulator Chroma 61845 to emulate the weak grid. The main circuit parameters of the grid-connected VSC are shown in Tab. I. The control parameters and steady-state values are presented in Tabl. II. In real-life applications, the dc source with variable input power may be used, such as a PV generator, where the steady-state values of the system will be changed by the input power fluctuations. In this case, the stability analysis may need to be performed at different operating points.

Using the state-space model in the dq-frame, it is able to identify the critical oscillation modes and tell the stability margin by checking the corresponding damping ratios. Based on the control parameters in Table II, the frequencies and damping ratios of different dynamic modes are shown in Fig. 14, the dynamic mode at ±37 Hz have negative damping ratios, which is unstable. However, these stability analysis is difficult to be verified in the grid dq-frame directly from the perspectives of both the measurement and the interpretation.

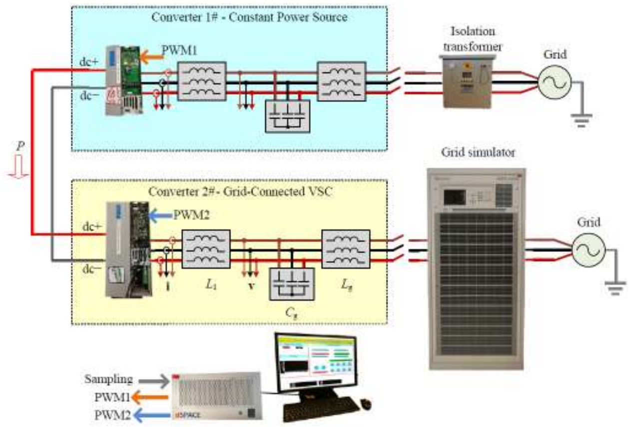

Fig. 13. Photo of the experimental setup.

TABLE I
MAIN CIRCUIT PARAMETERS OF GRID-CONNECTED VSC

	Parameters	Values
V_{dc}	Input dc-link voltage	600 V
V_1	Rated line to line grid voltage, RMS	126 V
f_1	Grid fundamental frequency	50 Hz
f_{sw}	Inverter switching frequency	10 kHz
f_s	Inverter control sampling frequency	10 kHz
P_n	Rated power	3050 W
C_{dc}	Dc-link capacitance	1500 μF
L_1	Inverter-side inductance	1 mH
R_1	ESR of the inverter-side inductor	0.3 mΩ
C_g	Equivalent grid-side capacitance	20 μF
R_{Cg}	ESR of the grid-side capacitor	0.5 mΩ
L_g	Equivalent grid-side inductance	11 mH
R_{Lg}	ESR of the grid-side inductor	3.3 mΩ

TABLE II
CONTROL PARAMETERS AND STEADY-STATE VALUES

	Parameters	Values
k_a	Proportional gain of the feedforward controller	1
ω_a	Corner frequency of the feedforward controller	12560
k_{pc}	Proportional gain of the ac current controller	5.236
k_{ic}	Integral gain of the ac current controller	1827
k_{pp}	Proportional gain of the PLL controller	1.392
k_{ip}	Integral gain of the PLL controller	122.4
k_{pd}	Proportional gain of the active power controller	0.095
k_{id}	Integral gain of the active power controller	2.998
k_{pa}	Proportional gain of the ac voltage controller	1.519
ω_{ac}	Corner frequency of the ac voltage controller	6.283
I_{d1}	Steady-state value ac current at d-axis	25 A
I_{q1}	Steady-state value ac current at q-axis	−9.6 A
V_{d1}	Steady-state value PCC voltage at d-axis	126 V
V_{q1}	Steady-state value PCC voltage at q-axis	0 V

On the one hand, the current and voltage oscillations can not measurable directly and the ideal phase angle θ_1 defined by the fundamental positive component of PCC voltage needs to be estimated for *dq*-transformation, which could be easily distorted by oscillation itself. Any algorithm that used to estimate θ_1 may introduce additional errors due to the dynamics of the phase-tracking controller and the filters used for separating the fundamental positive component of PCC voltage from oscillations. Fig. 15 and 16 show the oscillated voltage and current waveforms in the different grid *dq*-frame estimated by PLL with different control bandwidth. As seen, the oscillation magnitudes of voltages and currents are significantly different from each other in different estimated grid *dq*-frames.

On the other hand, the linkage between oscillation frequencies in the *dq*-frame and the *αβ*-frame is control-structure dependent. Considering the 50Hz frequency shift effect of the *dq* transformation, if the control system is symmetrical for *d*- and *q*-axis (such as single current control loop), 37 Hz oscillation in the *dq*-frame only results in single oscillation at 87 Hz in the *αβ*-frame [27]. If the control system is asymmetrical, then 37 Hz oscillation in the *dq* frame will result in 13 Hz and 87 in the *αβ*-frame. Therefore, it is not straightforward to predict the actual oscillations in the *αβ*-frame based on the modal analysis results in the *dq*-frame.

Using the state-space model in the *αβ*-frame, the frequencies and damping ratios of different dynamic modes can be directly obtained, as shown in Fig. 17, the dynamic modes at 13 Hz and 87 Hz have negative damping ratios, and thus they are unstable. Moreover, according to Eq. (78), the right eigenvectors of the two critical dynamic modes at 13 Hz and 87 Hz can be obtained, which provides an insight on the oscillations magnitudes of the PCC voltages and currents in the *αβ*-frame, as shown in Fig. 18. As seen, the oscillations in PCC voltages are dominated at 87 Hz, while comparable oscillations at both 13 Hz and 87 Hz are observed in the PCC currents. These analysis results can be directly verified in the *αβ*-frame.

Fig. 19 shows experimental results, where the sustained low-frequency oscillations can be observed in both the PCC voltages and currents. According to the DFT analysis in Fig. 20, the oscillation frequencies can be observed at 13 Hz and 87 Hz, and the normalized magnitudes of the oscillations are matched well with the predictions in Fig. 18.

Fig. 21 shows the damping ratio sensitivity of the critical modes at 13 Hz and 87 Hz with respect to the different controller parameters. It reveals that the tuning of the proportional gains k_{pp} in the PLL controller and k_{pc} in ac current controller is the most effective way to stabilize the unstable modes. As for the case in this paper, the control parameters k_{pp} and k_{pc} are set 0.8 and 1.2 of their original values, respectively. Fig. 22 shows the frequencies and damping ratios of dynamic modes in *αβ*-frame after tuning the controllers, where the unstable modes are successfully stabilized.

Fig. 23 shows the experimental results after tuning the controller parameters, and the system is stabilized, which confirms the effectiveness of the control tuning strategy.

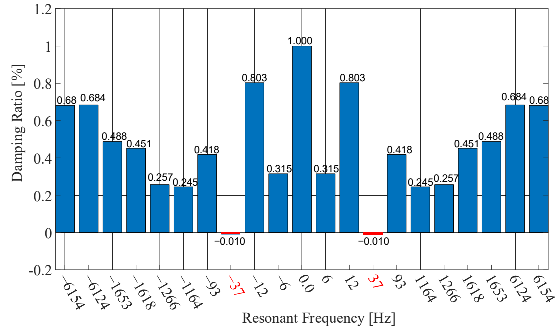

Fig. 14 Frequencies and damping ratios of dynamic modes in the ideal grid *dq*-frame

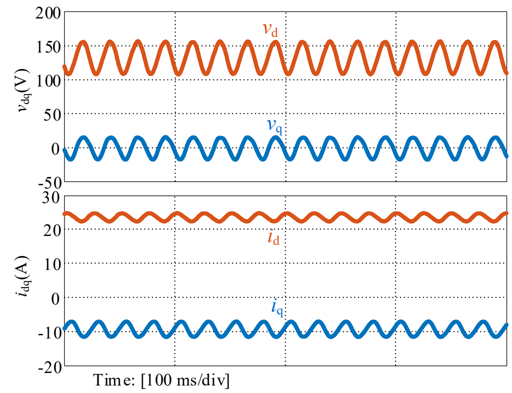

Fig. 15 Transformed waveforms in the grid *dq*-frame estimated by PLL with 20 Hz control bandwidth

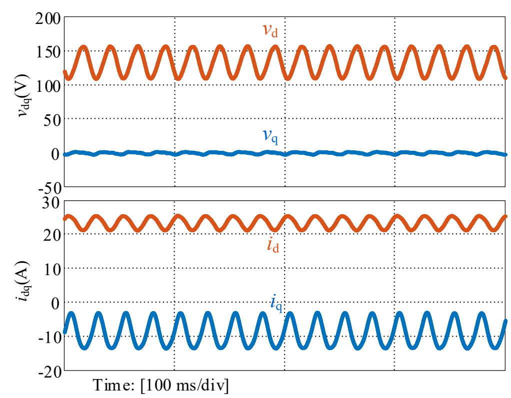

Fig. 16 Transformed waveforms in the grid *dq*-frame estimated by PLL with 100 Hz control bandwidth

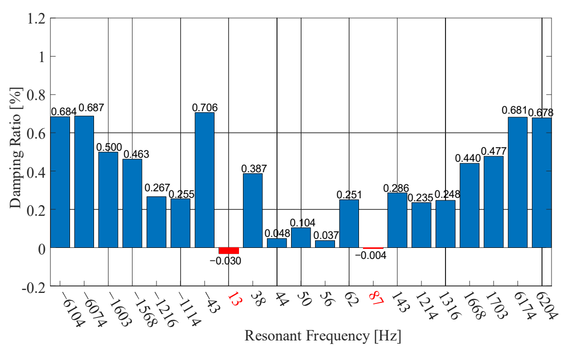

Fig. 17 Frequencies and damping ratios of dynamic modes in the *αβ*-frame

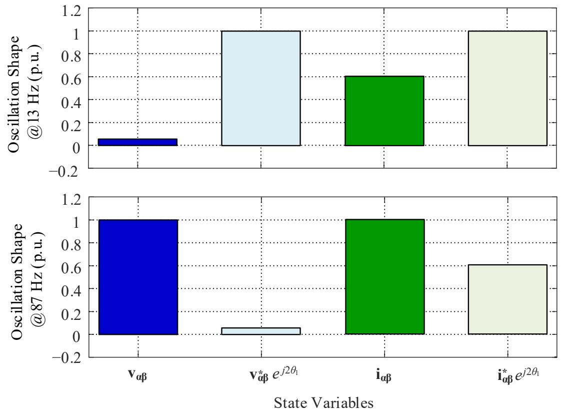

Fig. 18 Oscillations of PCC voltages and currents for unstable modes at 13 Hz and 87Hz in the $\alpha\beta$-frame

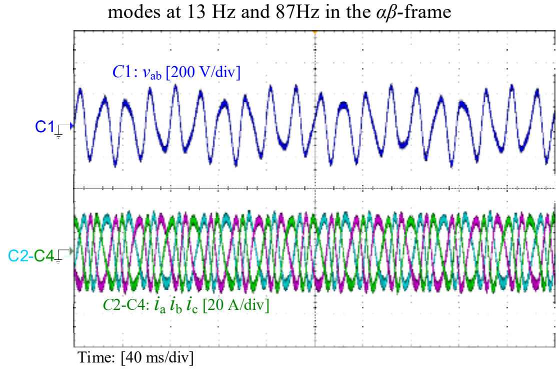

Fig. 19 Oscillated experimental waveforms in the $\alpha\beta$ frame.

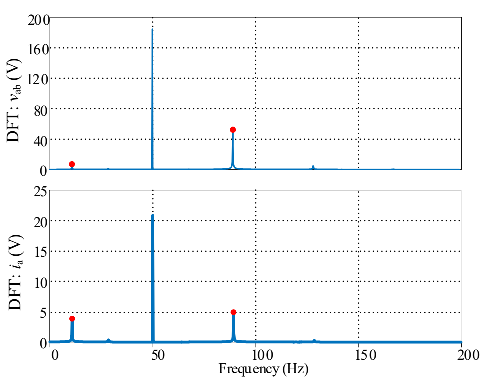

Fig. 20 DFT analysis experimental waveforms in the $\alpha\beta$ frame.

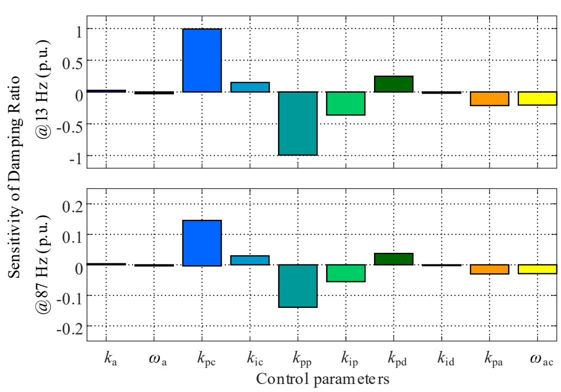

Fig. 21 Damping ratio sensitivity of the unstable modes and critical modes

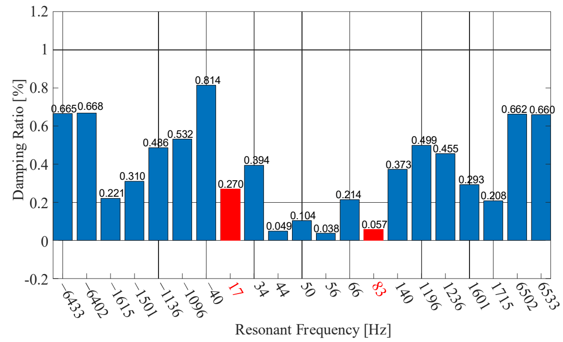

Fig. 22 Frequencies and damping ratios of dynamic modes in the $\alpha\beta$-frame after tuning the controllers.

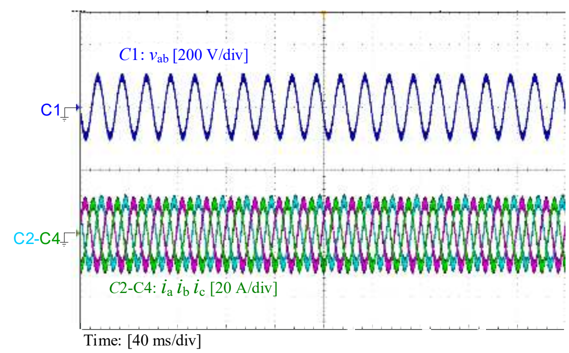

Fig. 23 Stabilized experimental waveforms after tuning controllers

IX. Conclusion

This paper proposed a modular state-space model of grid-connected voltage source converters, where the cross-couplings among various loops are identified and represented by the implicit interconnections, which allows the different control loops can be modeled separately and merged together like building blocks. Moreover, the mathematical relationship between the state-space models in the *dq*-frame and the *αβ*-frame is established. Intuitive interpretations of the modal analysis in the *αβ*-frame are also provided which can directly predict the frequencies and magnitudes of voltage and current oscillations in the *αβ*-frame. Experimental results from a 3kW VSC confirms the accuracy of the established state-space model and the effectiveness of the new modal analysis.

Appendix A

1. *AC current controller*

The inputs are *dq*-current errors i_{d_err}, i_{q_err} and the outputs are part of the PWM references, noted as v_{m1d}, v_{m1q}. Defining the states in integrators of current controllers $G_i(s)$ as γ_{id}, γ_{iq}, the state-space models of the current controllers can be given by:

$$\underbrace{\begin{bmatrix} \dot{\gamma}_{id} \\ \dot{\gamma}_{iq} \end{bmatrix}}_{\dot{\vec{x}}_1} = \underbrace{\begin{bmatrix} 0 & 0 \\ 0 & 0 \end{bmatrix}}_{F_1} \underbrace{\begin{bmatrix} \gamma_{id} \\ \gamma_{iq} \end{bmatrix}}_{\vec{x}_1} + \underbrace{\begin{bmatrix} 1 & 0 \\ 0 & 1 \end{bmatrix}}_{H_1} \underbrace{\begin{bmatrix} i_{d\_err} \\ i_{q\_err} \end{bmatrix}}_{\vec{a}_1} \tag{A1a}$$

$$\underbrace{\begin{bmatrix} v_{m1d} \\ v_{m1q} \end{bmatrix}}_{\vec{b}_1} = \underbrace{\begin{bmatrix} k_{ic} & 0 \\ 0 & k_{ic} \end{bmatrix}}_{J_1} \underbrace{\begin{bmatrix} \gamma_{id} \\ \gamma_{iq} \end{bmatrix}}_{\vec{x}_1} + \underbrace{\begin{bmatrix} k_{pc} & 0 \\ 0 & k_{pc} \end{bmatrix}}_{K_1} \underbrace{\begin{bmatrix} i_{d\_err} \\ i_{q\_err} \end{bmatrix}}_{\vec{a}_1} \tag{A1b}$$

2. *Feedforward Controller*

The inputs of the feedforward controller are PCC voltages $v_{\mathrm{d}}^{\mathrm{c}}, v_{\mathrm{q}}^{\mathrm{c}}$, and the outputs are PWM reference noted as $v_{\mathrm{m2d}}, v_{\mathrm{m2q}}$. By defining $[x_{\mathrm{ff\_d}}, x_{\mathrm{ff\_q}}]^{\mathrm{T}}$ as the state variables, the state-space model of feedforward controllers $G_{\mathrm{ff}}(s)$ can be derived as:

$$\underbrace{\begin{bmatrix} \dot{x}_{\mathrm{ff\_d}} \\ \dot{x}_{\mathrm{ff\_q}} \end{bmatrix}}_{\dot{\vec{x}}_2} = \underbrace{\begin{bmatrix} -\omega_{\mathrm{a}} & 0 \\ 0 & -\omega_{\mathrm{a}} \end{bmatrix}}_{F_2} \underbrace{\begin{bmatrix} x_{\mathrm{ff\_d}} \\ x_{\mathrm{ff\_q}} \end{bmatrix}}_{\vec{x}_2} + \underbrace{\begin{bmatrix} 1 & 0 \\ 0 & 1 \end{bmatrix}}_{H_2} \underbrace{\begin{bmatrix} v_{\mathrm{d}}^{\mathrm{c}} \\ v_{\mathrm{q}}^{\mathrm{c}} \end{bmatrix}}_{\vec{a}_2} \tag{A2a}$$

$$\underbrace{\begin{bmatrix} v_{\mathrm{m2d}} \\ v_{\mathrm{m2q}} \end{bmatrix}}_{\vec{b}_2} = \underbrace{\begin{bmatrix} -k_{\mathrm{a}}\omega_{\mathrm{a}} & 0 \\ 0 & -k_{\mathrm{a}}\omega_{\mathrm{a}} \end{bmatrix}}_{J_2} \underbrace{\begin{bmatrix} x_{\mathrm{ff\_d}} \\ x_{\mathrm{ff\_q}} \end{bmatrix}}_{\vec{x}_2} + \underbrace{\begin{bmatrix} k_{\mathrm{a}} & 0 \\ 0 & k_{\mathrm{a}} \end{bmatrix}}_{K_2} \underbrace{\begin{bmatrix} v_{\mathrm{d}}^{\mathrm{c}} \\ v_{\mathrm{q}}^{\mathrm{c}} \end{bmatrix}}_{\vec{a}_2} \tag{A2b}$$

3. *Digital Control Delay*

The inputs of the control delay are PWM references v_{md}, v_{mq}, and the outputs are VSC bridge voltages $v_{\mathrm{od}}, v_{\mathrm{oq}}$. By defining $[x_{\mathrm{del\_1d}}, x_{\mathrm{del\_2d}}, x_{\mathrm{del\_3d}}, x_{\mathrm{del\_1q}}, x_{\mathrm{del\_2q}}, x_{\mathrm{del\_3q}}]^{T}$ as the state variables, the state-space model of the control delay can be derived as:

$$\underbrace{\begin{bmatrix} \dot{x}_{\mathrm{del\_1d}} \\ \dot{x}_{\mathrm{del\_2d}} \\ \dot{x}_{\mathrm{del\_3d}} \\ \hline \dot{x}_{\mathrm{del\_1q}} \\ \dot{x}_{\mathrm{del\_2q}} \\ \dot{x}_{\mathrm{del\_3q}} \end{bmatrix}}_{\dot{\vec{x}}_3} = \underbrace{\left[\begin{array}{c|c} F_{\mathrm{d}} & 0 \\ \hline 0 & F_{\mathrm{q}} \end{array}\right]}_{F_3} \underbrace{\begin{bmatrix} x_{\mathrm{del\_1d}} \\ x_{\mathrm{del\_2d}} \\ x_{\mathrm{del\_3d}} \\ \hline x_{\mathrm{del\_1q}} \\ x_{\mathrm{del\_2q}} \\ x_{\mathrm{del\_3q}} \end{bmatrix}}_{\vec{x}_3} + \underbrace{\left[\begin{array}{c|c} H_{\mathrm{d}} & 0 \\ \hline 0 & H_{\mathrm{q}} \end{array}\right]}_{H_3} \underbrace{\begin{bmatrix} v_{\mathrm{md}} \\ \hline v_{\mathrm{mq}} \end{bmatrix}}_{\vec{a}_3} \tag{A3a}$$

$$\underbrace{\begin{bmatrix} v_{\mathrm{od}} \\ \hline v_{\mathrm{oq}} \end{bmatrix}}_{\vec{b}_3} = \underbrace{\left[\begin{array}{c|c} J_{\mathrm{d}} & 0 \\ \hline 0 & J_{\mathrm{q}} \end{array}\right]}_{J_3} \underbrace{\begin{bmatrix} x_{\mathrm{del\_1d}} \\ x_{\mathrm{del\_2d}} \\ x_{\mathrm{del\_3d}} \\ \hline x_{\mathrm{del\_1q}} \\ x_{\mathrm{del\_2q}} \\ x_{\mathrm{del\_3q}} \end{bmatrix}}_{\vec{x}_3} + \underbrace{\begin{bmatrix} -1 & 0 \\ 0 & -1 \end{bmatrix}}_{K_3} \underbrace{\begin{bmatrix} v_{\mathrm{md}} \\ \hline v_{\mathrm{mq}} \end{bmatrix}}_{\vec{a}_3} \tag{A3b}$$

where the matrices F_{d}, F_{q}, H_{d}, H_{q}, J_{d}, J_{q} are expressed by:

$$F_{\mathrm{d}} = F_{\mathrm{q}} = \begin{bmatrix} 0 & 1 & 0 \\ 0 & 0 & 1 \\ -120/T_{\mathrm{d}}^3 & -60/T_{\mathrm{d}}^2 & -12/T_{\mathrm{d}} \end{bmatrix} \tag{A4a}$$

$$H_{\mathrm{d}} = H_{\mathrm{q}} = \begin{bmatrix} 0 & 0 & 1 \end{bmatrix}^{T} \tag{A4b}$$

$$J_{\mathrm{d}} = J_{\mathrm{q}} = \begin{bmatrix} 240/T_{\mathrm{d}}^3 & 0 & 24/T_{\mathrm{d}} \end{bmatrix} \tag{A4c}$$

4. *L filter*

For the *L* filter, the relationship between the inductor voltages v_{Ld}, v_{Lq} and inductor currents $i_{\mathrm{d}}^{\mathrm{c}}, i_{\mathrm{q}}^{\mathrm{c}}$ in the time domain can be given by:

$$\frac{di_{\mathrm{d}}^{\mathrm{c}}}{dt} = \omega_1 i_{\mathrm{q}}^{\mathrm{c}} - \frac{R_1}{L_1} i_{\mathrm{d}}^{\mathrm{c}} + \frac{v_{\mathrm{Ld}}}{L_1} \tag{A5a}$$

$$\frac{di_{\mathrm{q}}^{\mathrm{c}}}{dt} = -\omega_1 i_{\mathrm{d}}^{\mathrm{c}} - \frac{R_1}{L_1} i_{\mathrm{q}}^{\mathrm{c}} + \frac{v_{\mathrm{Lq}}}{L_1} \tag{A5b}$$

Therefore, the state-space model of the *L* filter can be derived by:

$$\underbrace{\begin{bmatrix} \dot{i}_{\mathrm{d}}^{\mathrm{c}} \\ \dot{i}_{\mathrm{q}}^{\mathrm{c}} \end{bmatrix}}_{\dot{\vec{x}}_4} = \underbrace{\begin{bmatrix} -\dfrac{R_1}{L_1} & \omega_1 \\ -\omega_1 & -\dfrac{R_1}{L_1} \end{bmatrix}}_{F_4} \underbrace{\begin{bmatrix} i_{\mathrm{d}}^{\mathrm{c}} \\ i_{\mathrm{q}}^{\mathrm{c}} \end{bmatrix}}_{\vec{x}_4} + \underbrace{\begin{bmatrix} \dfrac{1}{L_1} & 0 \\ 0 & \dfrac{1}{L_1} \end{bmatrix}}_{H_4} \underbrace{\begin{bmatrix} v_{\mathrm{Ld}} \\ v_{\mathrm{Lq}} \end{bmatrix}}_{\vec{a}_4} \tag{A6a}$$

$$\underbrace{\begin{bmatrix} i_{\mathrm{d}}^{\mathrm{c}} \\ i_{\mathrm{q}}^{\mathrm{c}} \end{bmatrix}}_{\vec{b}_4} = \underbrace{\begin{bmatrix} 1 & 0 \\ 0 & 1 \end{bmatrix}}_{J_4} \underbrace{\begin{bmatrix} i_{\mathrm{d}}^{\mathrm{c}} \\ i_{\mathrm{q}}^{\mathrm{c}} \end{bmatrix}}_{\vec{x}_4} + \underbrace{\begin{bmatrix} 0 & 0 \\ 0 & 0 \end{bmatrix}}_{K_4} \underbrace{\begin{bmatrix} v_{\mathrm{Ld}} \\ v_{\mathrm{Lq}} \end{bmatrix}}_{\vec{a}_4} \tag{A6b}$$

REFERENCES

[1] F. Blaabjerg, Z. Chen, and S. B. Kjaer, “Power electronics as efficient interface in dispersed power generation systems,” *IEEE Trans. Power Electron*., vol. 19, no. 5, pp. 1184-1194, Sep. 2004.

[2] T. M. Jahns and V. Blasko, “Recent advances in power electronics technology for industrial and traction machine drives,” *IEEE Proc.*, vol. 89, no. 6, pp. 963-975, Jun. 2001.

[3] N. Flourentzou, V. G. Agelidis, and G. D. Demetriades, “VSC-based HVDC power transmission systems: an overvew,” *IEEE Trans. Power Electron*., vol. 24, no. 3, pp. 592-602, Mar. 2009.

[4] X. Wang, F. Blaabjerg, and W. Wu, “Modeling and analysis of harmonic stability in ac power-electronics-based power system,” *IEEE Trans. Power Electron.*, vol. 29, no. 12, pp. 6421-6432, Dec. 2014.

[5] J. Sun, “Impedance-based stability criterion for grid-connected inverters,” *IEEE Trans. Power Electron.*, vol. 26, no. 11, pp. 3075–3078, Nov., 2011.

[6] L. Harnefors, L. Zhang, andM. Bongiorno, “Frequency-domain passivity based current controller design,” *IET Power Electron.*, vol. 1, no. 4, pp. 455–465, Dec., 2008.

[7] D. Yang, X. Ruan, and H. Wu, “Impedance shaping of the grid-connected inverter with LCL filter to improve its adaptability to the weak grid condition,” *IEEE Trans. Power Electron*., vol. 29, no. 11, pp. 5795–5805, Nov., 2014.

[8] L. Harnefors, M. Bongiorno, and S. Lundberg, “Input-admittance calculation and shaping for controlled voltage-source converters,” *IEEE Trans. Ind. Electron.*, vol. 54, no. 6, pp. 3323–3334, Dec., 2007.

[9] M. Cespedes and J. Sun, “Impedance modeling and analysis of grid-connected voltage-source converters,” *IEEE Trans. Power Electron*., vol. 29, no. 3, pp. 1254–1261, Mar. 2014.

[10] L. Harnefors, “Modeling of three-phase dynamic systems using complex transfer functions and transfer matrices,” *IEEE Trans. Ind. Electron.*, vol. 54, no. 4, pp. 2239–2248, Aug. 2007.

[11] M. K. Bakhshizadeh, X. Wang, F. Blaabjerg, J. Hjerrild, L. Kocewiak, C. Leth Bak, B. Hesselbaek, “Couplings in Phase Domain Impedance Modelling of Grid-Connected Converters,” *IEEE Trans. Power Electron*., vol. 31, no. 10, pp. 6792–6796, Oct., 2016.

[12] Zhang, H., Wang, X., Harnefors, L., Gong, H., Hasler, J. P., & Nee, H. P. , “SISO Transfer Functions for Stability Analysis of Grid-Connected Voltage-Source Converters,” *IEEE Transactions on Industry Applications*, 55(3), 2931-2941.

[13] Y. Wang, X. Wang, F. Blaabjerg, and Z. Chen, “Harmonic Instability Assessment Using State-Space Modeling and Participation Analysis in Inverter-Fed Power Systems,” *IEEE Trans. Ind. Electron.*, vol. 64, no. 1, pp. 806–816, Jan. 2017.

[14] P. M. Anderson, B. L. Agrawal, and J. E. Van Ness, Subsynchronous Resonance in Power Systems, New York: IEEE Press, 1990.

[15] G. C. Verghese, I. J. Perezarriaga, and F. C. Schweppe, "Selective modal analysis with applications to electric power systems, part II: the dynamic stability problem," *IEEE Trans. Power Apparat. Syst*., vol. PAS-101, pp. 3126-3134, Sep. 1982.

[16] X. Wang and F. Blaabjerg, “Harmonic Stability in Power Electronic Based Power Systems: Concept, Modeling, and Analysis,” *IEEE Trans. Smart Grid*, 2018, Early access.

[17] N. Pogaku, M. Prodanovic, and T. C. Green, “Modeling, analysis and testing of autonomous operation of an inverter-based microgrid,” *IEEE Trans. Power Electron*., vol. 22, no. 2, pp. 613–625, Mar. 2007.

[18] L. Harnefors, X. Wang, A. G. Yepes and F. Blaabjerg, "Passivity-based stability assessment of grid-connected VSCs - an overview," *IEEE J. Emerg. Sel. Topics Power Electron.*, vol. 4, no. 1, pp. 116-125, Mar. 2016.

[19] R. Turner, S. Walton, and R. Duke, “A case study on the application of the Nyquist stability criterion as applied to interconnected loads and sources on grids,” *IEEE Trans. Ind. Electron.,* vol. 60, no. 7, pp. 2740- 2749, Jul. 2013.

[20] D. Yang, X. Wang, and F. Blaabjerg, "Sideband Harmonic Instability of Paralleled Inverters With Asynchronous Carriers," *IEEE Trans. Power Electron.*, vol. 33, no. 6, pp. 4571–4577, Jun. 2018.

[21] N. Kroutikova, C. A. Hernandez-Aramburo, and T. C. Green, "State-space model of grid-connected inverters under current control mode," *IET Electr. Power Appl.*, vol. 1, no. 3, p. 329, May, 2007.

[22] E. L. Duke, "Combining and connecting linear, multi-input, multi-output subsystem models." NASA Technical Memorandum, 1986, https://ntrs.nasa.gov/archive/nasa/casi.ntrs.nasa.gov/19860015695.pdf.

[23] G. Gaba, S. Lefebver, and D. Mukhedkar, "Comparative analysis and study of the dynamic stability of AC/DC systems," *IEEE Trans. Power Syst.*, vol. 3, no. 3, pp. 978-985, Aug. 1988.

[24] Y. Wang, X. Wang, Z. Chen, and F. Blaabjerg, "Small-Signal Stability Analysis of Inverter-Fed Power Systems Using Component Connection Method," *IEEE Trans. Smart Grid*, vol. 9, no. 5, pp. 5301–5310, Sep. 2018.

[25] M. Rasheduzzaman, J. A. Mueller, and J.W. Kimball, "An accurate small-signal model of inverter-dominated islanded microgrids using DQ reference frame," *IEEE J. Emerg. Sel. Topics Power Electron*., vol. 2, no. 4, pp. 1070–1080, Dec. 2014.

[26] H. Yi, X. Wang, F. Blaabjerg, and F. Zhuo, "Impedance Analysis of SOGI-FLL-Based Grid Synchronization," *IEEE Trans. Power Electron.*, vol. 32, no. 10, pp. 7409–7413, Oct. 2017.

[27] X. Wang, L. Harnefors, and F. Blaabjerg, "Unified impedance model of grid-connected voltage-source converters," *IEEE* Trans. *Power Electron.*, vol. 33, no. 2, pp. 1775–1787, Feb. 2018.

[28] M. Cespedes and J. Sun, "Impedance modeling and analysis of grid-connected voltage-source converters," *IEEE Trans. Power Electron*., vol. 29, no. 3, pp. 1254–1261, Mar. 2014.

[29] S. Shah and L. Parsa, "Impedance Modeling of Three-Phase Voltage Source Converters in DQ, Sequence, and Phasor Domains," *IEEE Trans. Energy Convers.*, vol. 32, no. 3, pp. 1139–1150, Sep. 2017.

[30] L. Harnefors, A. G. Yepes, A. Vidal, and J. Doval-Gandoy, "Passivity-Based Controller Design of Grid-Connected VSCs for Prevention of Electrical Resonance Instability," *IEEE Trans. Ind. Electron.*, vol. 62, no. 2, pp. 702–710, Feb. 2015.

[31] R. Ottersten, "On control of back-to-back converters and sensorless induction machine drives," Ph.D. dissertation, Dept. Elect. Power Eng., Chalmers Univ. Technol., Göteborg, Sweden, 2003.

[32] D. Yang, X. Wang, F. Blaabjerg, F. Liu, K. Xin, and Y. Liu, "Complex-Vector PLL for Enhanced Synchronization with Weak Power Grids," in *2018 IEEE 19th Workshop on Control and Modeling for Power Electronics* (*COMPEL*), 2018, pp. 1–6.

[33] G. Rogers, Power System Oscillations. Boston, MA: Springer US, 2000.

Dongsheng Yang (S'13–M'17–SM'19) received the B.S., M.S., and Ph.D. degrees in electrical engineering from Nanjing University of Aeronautics and Astronautics, Nanjing, China, in 2008, 2011, and 2016, respectively. In 2016, he joined Aalborg University, Aalborg, Denmark as a postdoc researcher, where he became the Assistant Professor in the Department of Energy Technology in 2018.

Since 2019, Dr. Yang has worked within the Electrical Energy Systems group at Eindhoven University of Technology (TU/e) as the Assistant Professor. His main research interests include modeling, analysis, and control of grid-interactive converters, harmonic and resonance mitigation of large-scale power electronics based power system, impedance measurement technique for real-field harmonic instability assessment, innovative hardware of power-electronics-based infrastructure for future power grids.

Xiongfei Wang (S'10-M'13-SM'17) received the B.S. degree from Yanshan University, Qinhuangdao, China, in 2006, the M.S. degree from Harbin Institute of Technology, Harbin, China, in 2008, both in electrical engineering, and the Ph.D. degree in energy technology from Aalborg University, Aalborg, Denmark, in 2013.

Since 2009, he has been with the Department of Energy Technology, Aalborg University, where he became an Assistant Professor in 2014, an Associate Professor in 2016, a Professor and Research Program Leader for Electronic Power Grid (eGrid) in 2018, and the Director of Aalborg University-Huawei Energy Innovation Center in 2020. His current research interests include modeling and control of grid-interactive power converters, stability and power quality of converter-based power systems, active and passive filters.

Dr. Wang was selected into Aalborg University Strategic Talent Management Program in 2016. He has received six IEEE Prize Paper Awards, the 2016 Outstanding Reviewer Award of IEEE Transactions on Power Electronics, the 2018 IEEE PELS Richard M. Bass Outstanding Young Power Electronics Engineer Award, the 2019 IEEE PELS Sustainable Energy Systems Technical Achievement Award, and the 2019 Highly Cited Researcher by Clarivate Analytics (former Thomson Reuters). He serves as a Member at Large for Administrative Committee of IEEE Power Electronics Society (2020-2022), and an Associate Editor for the IEEE Transactions on Power Electronics, the IEEE Transactions on Industry Applications, and the IEEE Journal of Emerging and Selected Topics in Power Electronics.